sciendo
Austrian Journal of Earth Sciences | Vienna | 2021 | Volume 114 | 66 - 87 | DOI: 10.17738/ajes.2021.0004

Microfacies and C/O-isotopes in lacustrine dolomites reflect variable environmental conditions in the Germanic Basin (Arnstadt Formation, Upper Triassic)

Barbara Hofbauer[1], Sebastian Viehmann[1,2], Susanne Gier[1], Stefano M. Bernasconi[3], Patrick Meister[1]*
1) Department of Geology, University of Vienna, Althanstr. 14, 1090 Vienna
2) Department of Lithospheric Research, University of Vienna, Althanstr. 14, 1090 Vienna
3) Geological Institute, ETH Zürich, Sonneggstr. 5, 8092 Zürich, Switzerland
*) Corresponding author: patrick.meister@univie.ac.at

KEYWORDS

Primary dolomite, Germanic Basin, playa lake, Arnstadt Formation, authigenic carbonates, microfacies

Abstract

The conditions in ancient evaporative environments conducive to authigenic carbonate (especially dolomite [$CaMg(CO_3)_2$]) formation are still insufficiently understood. Insights from microfacies analysis can help to constrain the conditions in these environments. We provide a brief overview of the microfacies association and carbon and oxygen isotope compositions of dolomite beds intercalated in a claystone-rich succession from the Norian Arnstadt Formation in Thuringia and Lower Saxony (Germany) in order to gain further insight into the depositional conditions and processes leading to the formation of authigenic Mg/Ca-carbonates in the Germanic Basin. The studied intervals are ascribed to lacustrine, partially evaporitic conditions, while the sedimentary structures were not obliterated by recrystallization. The microfacies of the dolomites is diverse, showing homogeneous micrite, mudclasts, lamination, and peloidal structures, and reflects a shallow to deeper water (below wave base) and episodically evaporative environment. The dolomites exhibit oxygen isotope values ($\delta^{18}O$) in the range from -5.21 to -0.36‰ VPDB and, hence, only represent a weak meteoric influence, suggesting that the authigenic carbonate generally formed under evaporative conditions. Carbon isotope values ($\delta^{13}C$) in the range of -4.28 to 1.39‰ VPDB indicate a small contribution of remineralized organic carbon, mainly in sediments that were presumably deposited in deeper water or under brackish conditions. Sedimentary structures, such as lamination with graded silt layers, reworked mudclasts embedded in a fine dolomicrite matrix, and peloids showing plastic deformation, indicate that the sediment was still unlithified. These observations would be consistent with an authigenic formation of Mg/Ca-carbonates directly from the lake water, and their deposition under variable conditions in a large playa-lake/perennial lake system.

1. Introduction

The formation of dolomite [$CaMg(CO_3)_2$] and other authigenic Ca/Mg-carbonates is commonly observed in modern evaporative lake environments (Peterson et al., 1963; Clayton et al., 1968; Eugster and Surdam, 1973; Eugster and Hardie, 1978; Last, 1990; Warren, 2000; Machel, 2004; Meister et al., 2011; Balci et al., 2016; McCormack et al., 2018; Fussmann et al., 2020). Whether these deposits serve as analogues for some of the dolomites in the geological record is, however, not always clear. Large amounts of dolomite may have formed by pervasive dolomitization during burial (Machel, 2004), while the Holocene environments simply may not have existed long enough to produce the same large accumulations of dolomite as in some examples from the geological record. For marine dolomites, there is petrographic and geochemical indication that some Triassic dolomites formed as early diagenetic or penecontemporaneous dolomite (i.e., dolomite that formed during or soon after deposition; e.g., Iannace and Frisia, 1994; Meister et al., 2013; Preto et al., 2015; Meister and Frisia, 2019). Rieder et al. (2019) show sedimentary structures that are indicative of soft sediment deformation, suggesting that the sediment was not lithified yet and that it was deposited as fine authigenic carbonate mud. Also, a few studies have suggested an early formation of ancient lacustrine dolomites (e.g., Last, 1990; Reinhard and Ricken, 2000; Yuan et al., 2015), but the question is, whether ancient lacustrine dolomites show similar sedimentary structures and microfacies assemblages as their marine counterparts.

The recent findings of preserved nano-crystalline structures in the Carnian Travenanzes Formation (Venetian Alps; Preto et al., 2015) and the Dolomia Principale (Brenta Dolomites, northern Italy; Meister and Frisia, 2019)

provide new evidence that support that some dolomites may indeed have formed as a primary precipitate. This interpretation is based on the assumption that structures in the range of a few nanometres are metastable and would not survive pervasive recrystallization. Dolomite formation via nanocrystal aggregation represents an intriguing hypothesis, which also would match with the observations of fine dolomite mud forming in the modern ephemeral lakes mentioned above. While nano-scale studies of ancient lacustrine dolomites are currently not available yet, and we do not know to what degree the authigenic Mg/Ca-carbonates were stoichiometric and well ordered, a sediment-petrographic study of lacustrine dolomite from the geological record could provide fundamental insight on the mode of formation and deposition of fine authigenic carbonate mud in ancient ephemeral and evaporative lake environments.

Dolomites of the Norian Arnstadt Formation (former Steinmergelkeuper; Beutler et al., 2005), Germany, have been suggested by Reinhard and Ricken (2000a) to have formed as a primary precipitate in a large perennial-lake/playa-lake system in the Germanic Basin. These authors provided a concept where dolomites are forming as part of cyclic sedimentation controlled by Milankovitch-scale variations in the monsoon effect on the continent. Since the Arnstadt Formation has only reached a moderate burial depth during its geological history of up to 1400 metres, including the overlying Jurassic units (Bachmann et al., 2002), while the supply of large quantities of cations (Mg) is probably reduced due to the embedding in thick claystone and marl deposits, there is a good chance that the carbonates were not overprinted by pervasive burial dolomitization, and primary sedimentary structures are still preserved.

While the depositional environment was entirely continental (Beutler et al., 1999; and references therein) and separated from the Tethyan realm by the Bohemian-Vindelician High, Keuper-type intercalations are frequently reported from the Alpine realm (e.g., Trümpy, 2006), where they occur as red clay-rich intercalations, also referred to as Carpathian Keuper. However, Keuper intercalations in the Alps tend to show strong tectonic overprint. Moreover, due to the scarcity of fossils, it is often difficult to distinguish marine influenced vs. playa lake deposits, such as in the Carnian Travenanzes Formation (Southern Alps; Rieder et al., 2019), showing a facies very similar to the lacustrine Arnstadt Formation. There, it was possible to derive a marine origin based on marine strontium isotope ratios (cf. Korte et al., 2003) as opposed to strongly radiogenic values that would indicate a continental origin of the ionic solutions. In comparison with Alpine facies dolomites, dolomites from the Arnstadt Formation offer the opportunity to investigate, whether lacustrine authigenic dolomites show similar sedimentological features as marine dolomites, and whether they display similar structures indicative of a primary authigenic formation in an ancient Triassic setting.

In the present study, we particularly focus on the assemblage of microfacies types, in comparison with Flügel's (2010) concept of standard microfacies types as well as limno-facies types. The samples were taken from the Arnstadt Formation in Lower Saxonia and Thuringia, from several stratigraphic sections. The dolomite layers clearly stand out in the red and gray claystone and marlstone successions, and their mineralogical composition was further analysed using X-ray diffraction. Stable carbon isotopes were measured to reveal the source of inorganic carbon and indicate the influence of microbial decomposition of organic matter. Oxygen isotopes were measured to trace the influence of meteoric water and/or the intensity of evaporation of the lacustrine brine. Based on the diversity of microfacies types, in accordance with their carbon and oxygen isotope signatures, we develop a simple microfacies model in the context of variable playa-lake/perennial lake conditions, conducive to primary precipitation and deposition of fine-grained Mg/Ca-carbonate.

2. Geological Setting

During the Triassic, the Germanic Basin had stabilized after the Palaeozoic orogenic phase, giving rise to a large epicontinental depositional environment, confined by the London-Brabant Massif to the west, the Fennoscandian High to the North and the Bohemian-Vindelician High to the east (Fig. 1a). The Germanic Basin (also called Central European Basin) was separated from the Tethys by the Bohemian-Vindelician High (Ziegler, 1990), and it shows a different geological evolution with a characteristic stratigraphic subdivision into Buntsandstein, Muschelkalk, and Keuper that reflect large-scale transgression and regression cycles (e.g., Aigner and Bachmann, 1992; Feist-Burkhardt et al., 2008).

The Buntsandstein Group consists of sandstones, conglomerates, and claystones in the southern part of the basin and more fine-grained, occasionally marine-brackish influenced sediments in the central parts (Bachmann et al., 2010). In the Middle Triassic Muschelkalk Group predominantly marine limestones were deposited in the central basin, while alluvial deposits are mainly provided from the north. Restricted conditions with evaporites and dolomites only occurred episodically in the south (e.g., Trigonodus dolomite; Bachmann et al., 2010; Schauer and Aigner, 1997).

The onset of the Keuper Group (Fig. 1b) was concurrent with a low sea level. The deposition of sandstones derived from the surrounding crystalline landmasses (Erfurt Formation), was followed by the Gipskeuper (comprising the lower and upper Gipskeuper, respectively the Grabfeld and Weser Formations), showing a more evaporative environment with the first playa-lake deposits as well as marine intercalations (Beutler et al., 1999; Beutler et al., 2005). The Gipskeuper sedimentation was interrupted by a pluvial episode, which provided the fluvial sandstones of the Stuttgart Formation (Kozur and Bachmann, 2010). The Gipskeuper deposits were overlain by the predominantly lacustrine Arnstadt Formation. Throughout the playa

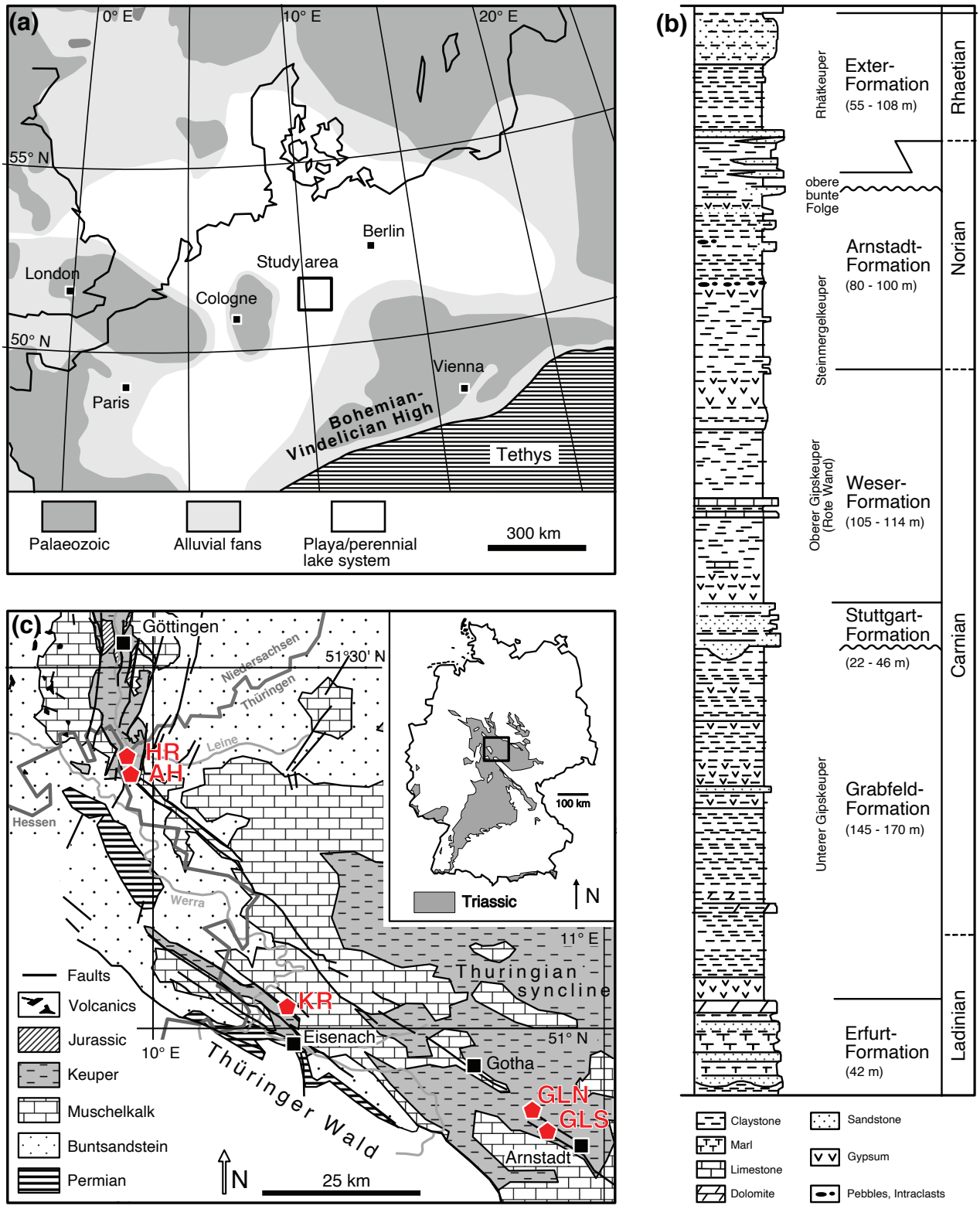

Figure 1: (a) Paleogeographic map with marked study area, showing the dimension of the depositional system. Modified after Ziegler (1990), as in Reinhard and Ricken (2000). (b) Ladinian-Rhaetian lithostratigraphy of the Germanic Basin, modified after Arp et al. (2004) and references therein. (c) Simplified geological map of the Leinetal Graben and the western part of the Thuringian Syncline (after Patzelt, 1994; Arp et al., 2004; and references therein), showing the outlines of the Arnstadt Formation and the locations of the studied sections (red points). HR – Hottenrode, AH – Altes Holz, KR – Krauthausen, GLN – Gleichen North, GLS – Gleichen South.

deposition in the central basin (Weser and Arnstadt Formations) a fluvial facies persisted along the basin margins, with coarse sandstones delivered from the Vindelician-Bohemina High (Steigerwald, Hassberge, Mainhardt, and Löwenstein Formations; also called "Sandsteinkeuper"; e.g. Beutler et al., 2005). Playa sedimentation declined with the Rhaetian transgression and associated marine-deltaic sandstones of the Exter Formation.

2.1 The Arnstadt Formation (Steinmergelkeuper)

The Arnstadt Formation consists mainly of fine-grained clastics (claystones) and intercalated, a few dm-thick dolomite beds with minor evaporites (Reinhardt and Ricken, 2000b). The Arnstadt Formation encompasses a time interval of approximately 20 Ma (Kozur and Weems, 2010) and can be divided into three intervals in its type area in Thuringia and adjacent parts of Lower Saxony (Naumann, 1911; Kellner, 1997; Franz, 2008):

The Lower Red Series consists of about 40 m of mudstone cycles of reddish-brown colour that were deposited in a playa lake system. Typical cycles include thin and stratified dolomitic claystones grading into massive dolomitic claystones. At the top, dolocrete layers can be found.

The Middle Grey Series has a thickness of about 30 m. It shows a cyclicity that is best pronounced at the bottom and the top of the series, caused by fluctuating salinities in a perennial lake system, as evidenced by freshwater bivalves and fish scales (Arp et al., 2005). Typical lithologies are greenish-grey layered mudstones with thin intercalated dolomicrite beds. These sediments were deposited in perennial lakes with fluctuating salinities.

The Upper Red Series is around 30 m thick with greenish to reddish siltstones and dolomitic claystones and rare intercalated dolomite beds as indication of temporary playa lake systems. An unconformity overlain by reworked clasts and oncoids within the Upper Red Series (conglomerate; Arp et al., 2005) marks the transition to a meandering fluvial system with sand-, silt-, and dolomitic claystones. The upper boundary of the Arnstadt Formation to the Exter Formation is drawn at the transition from reddish to greenish-grey sediments (Arp et al., 2005).

While this threefold division occurs in Thuringia, grey claystone marl occurs throughout the Arnstadt Formation in Pomerania and the Red Series prevails in central Poland (Franz, 2008; Barnasch, 2010; Barth et al., 2018). The pronounced cyclicity has been described by Duchrow (1984), Beutler et al. (1999), Reinhardt (2000), and Reinhardt and Ricken (2000a, b), whereby the stacking pattern was mainly related to Milankovich precession cycles at the metre scale (Vollmer, 2005). According to their hypothesis, dolomites form periodically during lake-level highstands that were followed by lake-level lowstands and erosion.

2.2 Study Area

The studied sections are located in Lower Saxony and Thuringia (Fig. 1c). A thick succession of Zechstein and the typical Triassic sediments of the Germanic Basin (Buntsandstein, Muschelkalk, Keuper) covering a Variscan basement characterize the geology (Stille and Lotze, 1932, 1933; Arp et al., 2004). A prominent structural element in the area is the Leinetal Graben, an N-S striking rift zone of approximately 48 km length. Keuper sediments crop out in the graben, whereas Buntsandstein, Muschelkalk, and some volcanic rocks of Tertiary age are present on the surrounding scarplands. Outcrops are rare in the study area, due to low erosion resistance of the Keuper sediments, but they do occur in quarries and along roadcuts.

3. Methods

Stratigraphic sections were measured at the slope of a forest road at Altes Holz near Bornhagen (51.379694/9.931722), a clay pit near Hottenrode (51.379698/9.931719; Arp et al., 2004) and a clay pit near Ütterröda (community of Krauthausen; 51.029554/10.287320; Fig. 1c). Samples were also collected at two natural outcrops near Burg Gleichen (Thurungia; 50.885029/10.842556; and 50.879829/10.836588). In total, 19 samples (both carbonate beds and claystone) were collected. Thin section analysis was carried out using a Leica DM 2700 P light microscope. The petrography was described using the nomenclatures of Dunham (1962) and Folk (1959) and was assigned to standard microfacies types (SMF) and lacustrine microfacies types (LMF), respectively, after Flügel (2010). Crystallization textures were further determined using the classifications of Friedman (1965).

For SEM analysis the thin sections were first polished with SiC powder (0.25 µm grain size), then with Logitech Syton SF1 colloidal silica (pH 10; 0.032 µm grain size; Logitech Ltd., Old Kilpatrick, Glasgow, G60 5EU, UK). The polished sections were coated with carbon and analysed with a FEI Inspect S50 SEM (Thermo Fisher Scientific, Bremen, Germany) in backscatter mode and electron dispersive X-ray (EDAX Ametek, New Jersey, U.S.A.) at the University of Vienna. Images were taken at a voltage of 10 kV, spot size 5, and a working distance of 10 mm.

Mineralogical analyses of whole rock powder were conducted with a PANalytical X'Pert PRO X-ray diffractometer (Malvern Panalytical, Almelo, The Netherlands) with CuKα-radiation (40 kV, 40 mA, step size 0.0167, 2-70°, 5 s per step). The X-ray diffraction patterns were interpreted using the Panalytical software "X'Pert High score plus". The stoichiometric composition of the dolomite was determined from the shift of the 104 peak using the equation of Lumsden (1979), and the structural order is indicated by the ratio of the peak heights of the (015) superlattice ordering peak to the (110) ordering peak (Füchtbauer and Goldschmidt, 1966).

Carbonate samples for stable carbon and oxygen isotopes were collected from thin section cuttings using a micro-drill. They were measured with a Delta V Plus mass spectrometer linked to a GasBench II (Thermo Fisher Scientific) at ETH Zürich (Zürich, Switzerland) following the procedure described in Breitenbach and Bernasconi (2011). Values are reported in permil relative to the Vienna Peedee Belemnite (VPDB) standard. The precision was better than 0.1‰ for both isotopes. The oxygen isotope values were corrected for kinetic fractionation during dissolution of dolomite in anhydrous phosphoric acid at 70°C, using a fractionation factor of 1.009926 (Rosenbaum and Sheppard, 1986).

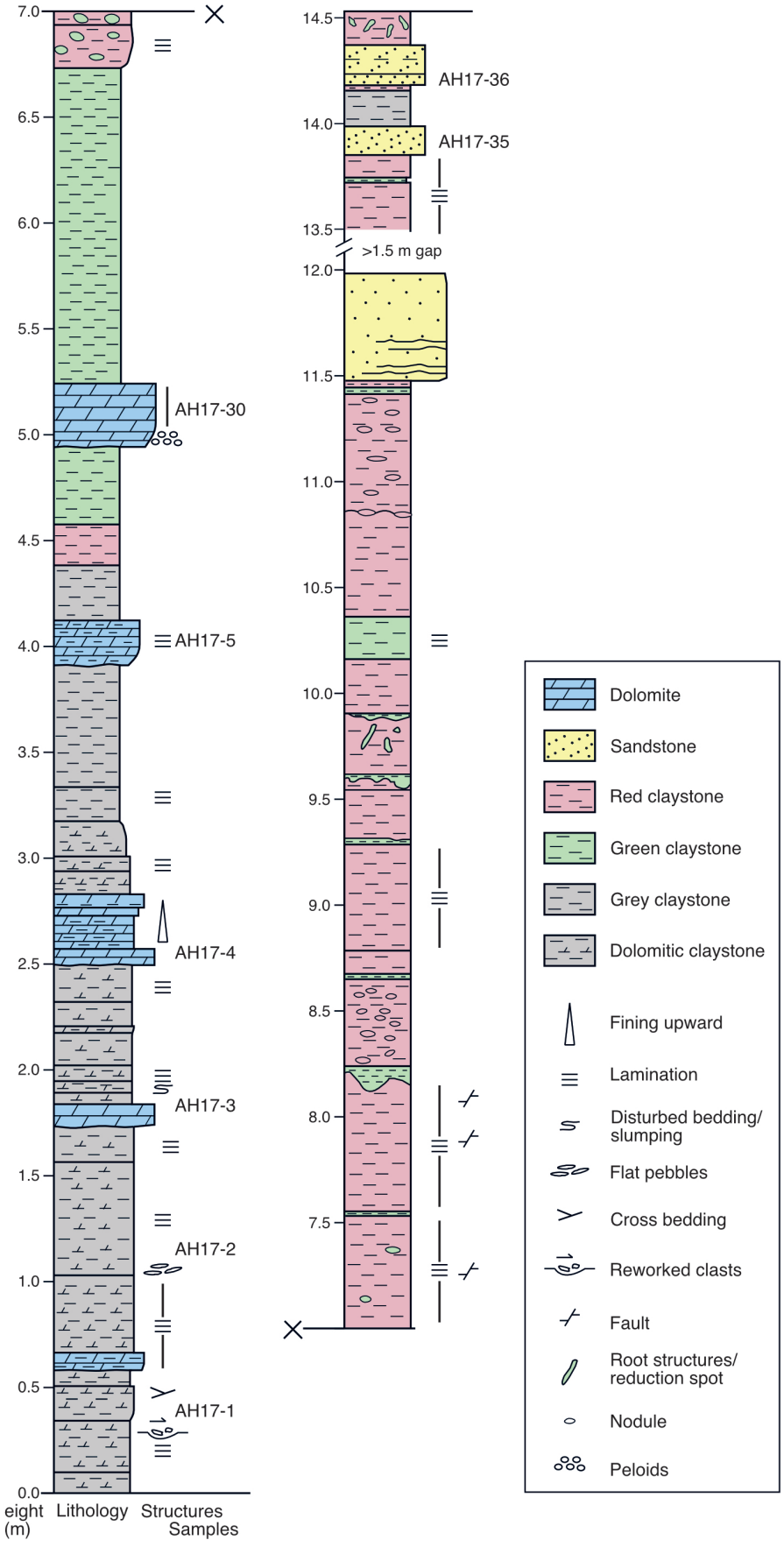

Figure 2: Stratigraphic section at Altes Holz near Bornhagen showing dolomite beds intercalated in clay-rich laminated or homogeneous dolomitic claystones. Sediment colours change from grey to red and green as indicated in the column left to the lithological column. Sample numbers are indicated as AH17-no. on the right side of the lithological column.

4. Results

4.1 Measured stratigraphic sections

Altes Holz/Bornhagen

In the lower five metres of the section Altes Holz (Fig. 2), grey to dark grey, macroscopically homogenous and laminated dolomitic claystone occurs (Samples AH17-1, 0.3 m; AH17-2, 1.15 m; Fig. 3a). The laminae appear to be due to intercalations of coarser (grain size >1 mm), detrital deposits. Light grey, 8 to 20-cm-thick dolomite beds are intercalated in the clay-rich sediments at the metre scale (Sample AH17-3, 1.8 m; and Sample AH17-4, 2.5 m; Figs 3b, c). The dolomite beds generally consist of one or a few massive beds underlain by thinner and irregular or nodular beds. The lower boundary of the dolomite beds is usually gradual whereas the boundary at the top is sharp. Thin, cm-scale bedding may occur at the transition to the dolomitic claystone. A sandstone bed at 3.9 m shows fine mm- to cm-scale lamination (sample AH17-5).

Above ca. 4 m, red shale with green horizons and reduction spots occur (Fig. 3d), with only one dolomite bed at 5.02 m (Sample AH17-30). The dolomite bed is associated with greenish claystones (Fig. 3d). Two sandstone beds with cross-bedding occur at 13.9 and 14.3 m, respectively (Samples AH17-35 and AH17-36).

Hottenrode

An 8.5-m-thick section was measured at Hottenrode, which consists of laminated siltstone, reddish and greenish claystone with intercalated sandstone beds. A dolomite bed is present at the base of the section, showing tectonic fracturing and strong lateral variation in thickness to more than a metre, possibly as a result of synsedimentary deformation. The dolomite is overlain by ca. 30 cm of yellowish claystone, where near the top a 2-cm-thick black, carbonaceous bed is intercalated (arrow in Fig. 3e). The claystone is covered by a >10-cm-thick polymictic dolomitic conglomerate ("C" in Fig. 3e). The grain size is between 1 mm and 2 cm, with well-rounded clasts of homogeneous, light coloured dolomite, as it typically occurs in the Arnstadt Formation. The conglomerate further contains dark dolomite clasts as well as carbonaceous plant debris. Fossil remains, including vertebrate bones and fresh-water shark teeth, are reported from this bed (Arp et al., 2004). Above the conglomerate, variable fluvial and lacustrine sediments are deposited.

Krauthausen

At the Krauthausen outcrop an 11.2-m-thick interval of claystone in the Lower Red Series (Patzelt, 1994) was measured. The claystones have a reddish, greenish, greyish, dark grey or violet colour and are either homogenous or laminated (Fig. 3f). Most light grey and greenish dm-scale bands are uncemented, but one hard cemented carbonate bed occurs at 5.63-5.78 m (arrow in Fig. 3f). In the hand specimen, this bed shows lamination and slumping.

Burg Gleichen

The outcrops southwest and north of Burg Gleichen include parts of the red series. Although the bedrock is largely covered by rubble or grass, and the stratigraphic context is difficult to recognize, single dolomitic beds clearly stand out. Most dolomite beds are light grey and fine-grained homogeneous. Sample GLN17-1 is from a greenish dolomitic sandstone bed with cross-bedding.

4.2 Petrography and microfacies

Homogenous (dolo)mudstone

Dolomicrite consists of homogeneous microcrystalline dolomite with a crystal size of less than 4 µm. Homogeneous dolomudstone (as a fabric; after Dunham, 1962) consists almost entirely of dolomicrite matrix (Fig. 4a), with only slight variations in colour, which is generally more brownish with increasing clay content. Some randomly distributed detrital mineral grains are mainly angular quartz at the few micrometre scale. Homogeneous dolomudstone occurs in the samples from the Burg Gleichen and in the dolomite beds from the lower grey series of Altes Holz. Also, cm-scale laminae in dolomitic claystone may consist of homogeneous dolomudstone. The homogeneous dolomudstone matches the limestone standard microfacies SMF 23 (non-laminated homogeneous micrite and microsparite without fossils) and the lacustrine microfacies type LMF 1 ("lime mudstone consisting of very fine-grained micrite crystals") after Flügel (2010), even though the carbonate phase is dolomite rather than calcite.

Laminated (dolo)mudstone

Some dolomites show a dolomicrite matrix with a lamination <100 µm to 1 mm (Figs 4b, c). The lamination is due to variation in colour, probably as a result of variations in grain size (Fig. 4b). Some laminae show silty layers, consisting of detrital quartz above a sharp boundary at the base, and they are fining-upward (Fig. 4c), grading into dolomicrite and dolomitic clay. Most lamination occurs in mixed siliciclastic sediments, such as in the Middle Grey Series of Altes Holz, and they resemble sandstone beds from the top of Altes Holz or from carbonate cemented sandstone from Burg Gleichen. Quartz laminae typically show cross-bedding (Fig. 4d). The dolomite bed of Krauthausen also shows lamination, which is mainly due to oncoid interlayers (see below). The laminae are sometimes deformed or torn and show slumping structures (Fig. 4e) or upward directed fluid escape (or pseudoteepee) structures (Fig. 4f). Laminated dolomudstone mainly falls within SMF 25 ("laminated evaporite-carbonate mudstone") and LMF 2 ("inhomogeneous laminated lime mudstone with very rare or no fossils"), although the carbonate phase is dolomite.

Intraclastic dolowackestone and rudstone

Dolomicrite mudclasts are often embedded in dolomicrite matrix, showing a matrix-supported fabric, i.e.,

wackestone (Fig. 5a). The mudclasts are commonly rounded or may have an irregular shape, or they are squeezed together and show ductile deformation. Also typically the homogenous dolomudstone shows a nodular structure apparently resulting from internal deformation (Fig. 5b; Sample AH17-4). These features occur at all of the sites within homogeneous dolomite beds, in particular in dolomites from the Grey Series at Altes Holz and in the conglomerate from Hottenrode. Mostly the mudclasts stand out due to either lighter or darker colour. The transition between dolo-wackestone and laminated dolomudstone is commonly along erosional surfaces, where clasts of the underlying micrite matrix are reworked and incorporated as rip-up clasts in the overlying micrite matrix (Figure 5c, d; Samples AH17-4 and KR17-1). Larger flat pebbles may exhibit a faint <100-µm-scale lamination (Fig. 5e; Sample AH17-3). Intraclastic wackestone also best fits to SMF 23 ("non-laminated homogeneous micrite and microsparite without fossils") while for the limnofacies LMF 3 ("Lime mudstone and wackestone with leaves of plants accumulated on bedding planes") and LMF 4 ("inhomogeneous fine-bedded intraclast wackestone characterized by reworked laminated mudstone of LMF 2 and nektonic fossils") would apply best, although fossils are rare.

The sample of the conglomerate from Hottenrode contains a diverse variety of clasts, including sandstone, pyrite as well as dolomicritic clasts and moulds of dissolved bioclasts. The grain-size spectrum is large and clasts are often arranged in a chaotic way, partially matrix supported and partially grain supported (Fig. 5f). The lithology is largely a lithoclastic rudstone and best fits to SMF 24 ("Lithoclastic floatstone, rudstone or breccia") or LMF 13 ("Lithobioclast rudstone"), respectively.

Peloidal grainstone

The dolomite bed at 5.02 m in the Altes Holz section (Sample AH17-30) shows a densely packed peloidal fabric. The peloids consist of homogeneous dolomicrite and are surrounded by an isopacheous cement rim (Fig. 6a). Peloids occur in different shapes and sizes (Fig. 6a). Matrix between the peloids is almost entirely absent, peloids even seem partially deformed to fill the space entirely. Besides peloids also elongate components occur (Fig. 6b), but all grains are surrounded by a thin rim of cement (Figs 6a-c). Peloids are also observed in the dolomite bed of Krauthausen, where they seem to be largely diffuse and amalgamated (Figure 6d, arrow). A crystal fan structure is superimposed on the peloidal structure in one lamina (labelled "fan" in Fig. 6d). Besides peloids, also various coated grains are observed (Fig. 6d; see below).

SEM images show further details of the peloidal structure in the dolomite bed from Altes Holz. Peloids are densely packed (Fig. 7a) with hardly any matrix in between. The bright mineral phase in the interstices was identified as barite (containing Ba and S) by EDX. At higher contrast, backscatter imaging reveals orientation contrast and thus provides insight into the shape and orientation of the crystals. The peloids consist of micron-scale mostly subhedral dolomite crystals showing random crystallographic orientation (Fig. 7b), which is typical for a (dolo) micrite. The matrix between the peloids, if present, shows coarser euhedral dolomite crystals. At higher magnification (Figs 7c, d), the radial arrangement of crystals in the cement rim is visible. Interestingly, the peloid in Figure 7c shows two cement rims and a central cavity, which looks like an ooid that was partially dissolved and the cavities became filled with dolomitic cement.

The grain-supported peloidal structure with sparitic matrix pertains to a peloidal grainstone, according to the classification of Dunham (1962). It fits best with SMF 16 ("Peloid grainstone and packstone") and according to lacustrine microfacies types partially falls into LMF 5 ("densely packed nodular, peloidal wackestone or floatstone with reworked lacustrine grains and with black pebbles of lacustrine limestone, sometimes also with extraclasts") with the carbonate phase being dolomite.

Ooid/onkoid packstone

Layers of coated grains, showing somewhat irregular shape with a truncated concentric structure, are observed in the dolomite bed from the Krauthausen outcrop (Sample KR17-1, 5.6 m; Figure 6e). The layers of oncoids are largely grain supported and show depositional structures, such as layering and imbrication. They were already lithified at the time of deposition, since they do not show deformation and they deform the adjacent clay layers. In limnic systems only LMF 10 applies to "oncoid packstone and wackestone". According to Flügel (2010), microoncoids may have nuclei of "quartz or silt grains, surrounded by only a few micritic laminae". No ooids are mentioned in the LMF classification by Flügel (2010).

4.3 X-ray diffraction

X-ray diffraction (Tab. 1; Fig. 8) showed that hard carbonate beds, recognized in the field, contain dolomite as the only carbonate phase. The dolomite is stoichiometric with an average of 49.8 ±0.43 mol% CaCO3. Also, a high structural ordering is indicated by an average 015/110-peak height ratio of 0.514 ±0.033. Other minerals include quartz, albite, K-feldspar and clay minerals, including chlorite, illite and smectite-illite mixed-layer clay minerals. Hematite was specifically recorded in samples with very low carbonate contents AH17-5 and AH17-35 (3.9 m and 12.2 m at Altes Holz). Laminated clay-rich beds between the hard beds in the middle grey series at Altes Holz are also rich in dolomite. Only one dolomite-rich layer occurred in the upper red/green series at Altes Holz (5 m). The carbonate fraction is dolomite in all samples from Burg Gleichen outcrops, and one bed sampled from the Krauthausen outcrop.

4.4 Carbon and oxygen isotope values

Carbon isotope values in the analysed carbonates are in the range of -4.28 to +1.39‰ VPDB and oxygen isotopes are in the range of -5.21 to -0.36‰ (Tab. 2; Fig. 9). Homogeneous and peloidal dolomites from the Red Series (Altes

Table 1: Results of XRD analysis of bulk samples from the Arnstadt Formation, from Altes Holz, Hottenrode, Krauthausen and Burg Gleichen outcrops. From left to right: Intensities of the quartz (101) peak and the dolomite (104) peak, dolomite 015/110-peak ratio (after Füchtbauer and Goldschmidt) and mole fraction of Ca in dolomite calculated from the shift of the 104 peak (Lumsden, 1979). All minerals present in the samples are listed with the order of decreasing abundance.

Sample	Position (m)	Quartz 101 cts	Dolomite 104 cts	Peak ratio 015/110	Stoichiometry Ca/(Ca+Mg)	Mineralogy
AH-17-1	0.33	968	7324	0.56	50.0	dolomite, quartz, clay minerals (chlorite, illite, smectite?)
AH-17-2	1.15	1336	6222	0.49	49.8	dolomite, quartz, clay minerals (chlorite, illite, smectite?)
AH17-3o	1.8	1680	5636	0.49	50.2	dolomite, quartz, clay minerals (chlorite, illite, smectite?)
AH-17-3u	1.8	1108	7135	0.49	49.8	dolomite, quartz, clay minerals (chlorite, illite)
AH-17-4	2.5	799	7109	0.50	49.9	dolomite, quartz, clay minerals (chlorite, illite)
AH-17-5a	3.99	7056	455		50.4	quartz, albite, k-fsp, dolomite, hematite, clay minerals (chlorite, illite, mixed layer)
AH-17-5b	3.99	4997	169		50.5	quartz, albite, k-fsp, dolomite, hematite, clay minerals (chlorite, illite, mixed layer)
AH-17-5c	3.99	10079				quartz, albite, k-fsp, hematite, clay minerals (chlorite, illite, mixed layer)
AH-17-30	5.02	856	8382	0.50	50.4	dolomite, quartz, albite, barite, clay minerals (chlorite)
AH-17-35o	13.9	13878				quartz, albite, hematite?, clay minerals (chlorite, illite)
AH-17-35u	13.9	15626				quartz, albite, hematite, clay minerals (chlorite, illite)
GLN-17-1	-	16034	903			quartz, albite, k-fsp, dolomite, calcite, clay minerals (illite?)
GLN2-17-1	-	1816	8690	0.49	49.9	dolomite, quartz, clay minerals (chlorite, illite, mixed layer)
GLN2-17-2	-	1890	8155	0.51	49.9	dolomite, quartz, clay minerals (chlorite, illite, mixed layer)
GLN2-17-3	-	684	7972	0.53	48.9	dolomite, quartz, clay minerals (chlorite, illite)
GLS17-1	-	2160	7431		50.2	dolomite, quartz, albite, k-fsp, clay minerals (illite)
GLS17-2	-	471	8587	0.59	50.2	dolomite, quartz, albite, clay minerals (illite)
GLS17-3	-	684	7972	0.53	48.9	dolomite, quartz, clay minerals (chlorite, illite, mixed layer)
GLS17-4	-	2148	7058	0.48	49.8	dolomite, quartz, clay minerals (chlorite, illite, mixed layer)
KR-17-1	5.63-5.78	2500	7573	0.55	49.9	dolomite, quartz, albite, k-fsp, clay minerals (illite)

Holz and Burg Gleichen), generally show a larger variation in $\delta^{18}O$ between -4.5 and +0.35‰, and also the most negative value of -6‰ (blue circles) is from a carbonate cemented sandstone in the Red Series (Altes Holz). Uncoupling of $\delta^{18}O$ from $\delta^{13}C$ is most prominent in peloidal dolomites from one single dolomite bed (AH17-30; green symbols in Fig. 9). Samples taken from mud clasts (brown symbols) show the widest range with $\delta^{13}C$ values between -4.3 and -2‰ while most $\delta^{18}O$ values remain near -2‰. The samples taken from dark grey dolomicrite intraclasts from the conglomerate at Hottenrode show the most negative $\delta^{13}C$ values of ca. -4‰. Least variable are laminated dolomites from the Grey Series (Altes Holz), which cluster around a $\delta^{18}O$ of -3‰ and a $\delta^{13}C$ of -2‰.

5. Discussion

5.1 Reconstruction of the depositional environment

The up to 20-cm-thick, intercalated dolomite beds represent episodes of modified environmental conditions, and therefore, the assigned microfacies types are only valid for the dolomite beds. Nevertheless, these microfacies types are to understand within the dynamics of cyclic deposition of carbonates within an otherwise siliciclastic dominated depositional system. Despite the monotonous appearance of the dolomite beds, thin section analysis reveals a remarkable diversity of microfacies within the large-scale facies distribution in the basin (cf. Franz, 2008; Barnasch, 2010). Based on the observation of our microfacies study, in accordance with information from the literature, we developed a facies model for the playa-lake/perennial-lake system as shown in Figures 10a-c.

Homogeneous dolomudstone fits to SMF 23 ("Non-laminated homogeneous micrite and microsparite without fossils"), indicating "deposition in a saline or evaporitic environments, e.g., in tidal ponds" (Flügel, 2010). As the conditions during deposition of the Arnstadt Formation were non-marine, tidal ponds can be excluded, and precipitation in a shallow ephemeral lake appears appropriate. The limnofacies fits best to LMF 1 ("Lime mudstone consisting of very fine-grained micrite crystals"). Flügel (2010) mentions that fine mud may originate from cyanobacterial and algal blooms as well as from abrasion of limestone, however, a primary precipitation may also occur, in particular under evaporative lake conditions (as further discussed below). In analogy with modern playa lakes, showing typically authigenic Ca/Mg-carbonate (also dolomite) formation (e.g., Last, 1990; Meister et al., 2011; McCormack et al., 2018; Fussmann et al., 2020), carbonates in the Arnstadt Formation are also likely authigenic. Due to the scarcity of organisms, it is unlikely that the sediment was bioturbated, however, homogenization is also observed in modern shallow-water lakes (see examples above) due to wave action, in particular if the sediment consists of very fine-grained carbonate mud. Disperse detrital clasts and mudclasts support the interpretation that the sediment was well mixed. Homogeneous dolomudstone is clearly associated with the Red Series, which is in line with previous interpretations as playa lake deposits (e.g., Reinhardt and Ricken, 2000b).

Laminated dolomudstone would fit to SMF 25 ("laminated evaporite-carbonate mudstone"), which, according to Flügel (2010), is typical to "upper intertidal to supratidal sabkha facies in arid and semiarid coastal plains and evaporitic lacustrine basins". However, an alternation of fine-crystalline dolomite, and diagenetically deformed layers with evaporite crystals (gypsum) is not observed in the studied samples. Rather, the lamination consists of graded laminae, some with a detrital quartz layer at the base and grading into clay-rich dolomite mudstone, truncated by an erosion surface. Teepee structures are only rarely observed. Despite similarities to SMF 25, the laminated dolomudstones are fundamentally different from those observed in the Travenanzes Formation. There, laminated mudstones are clearly supratidal, showing more features of evaporation, such as teepee structures and pseudomorphs after evaporites, and they were assigned to SMF 25 (see Rieder et al., 2019). Apparently, lamination is also preserved if essentially no water column is present to develop any significant water energy to homogenize the sediment. Lacustrine systems essentially lack the analogue to SMF 25, possibly because lakes do not usually show a large intertidal zone. The limnofacies most applicable to the laminated dolomudstones would be LMF 2 ("inhomogeneous laminated lime mudstone with very rare or no fossils"), including alternation of light and dark layers, where the dark layers are enriched in organic matter, as well as clay and silt-sized terrigenous quartz as part of the lamination. In contrast to SMF 25, LMF 2 is interpreted to reflect "a relatively deep and quiet-water basin", where the lamination is preserved, and a "stratified water column" is preventing bioturbation of the sediment. LMF 2 may better be applied to the laminated dolomudstones, in particular, since they occur in the Grey Series in the lower part of the Altes Holz section. Also in deep water deposits, lamination may reflect seasonal variations in sediment input, possibly due to episodically high water energy of flooding events and deep-water density currents. Alternatively, lamination may also be preserved in sheltered areas in shallow water, where stagnant conditions prevail in a palustrine environment. Pseudo-teepee structures as shown in Figure 4f may result from both syneresis and fluid escape at greater water depth or due to desiccation cracks in a shallow ephemeral lake, but they are only rarely observed in the studied samples.

Not observed at our study sites, but reported in the literature from other locations in the Arnstadt Formation (e.g., at the outcrop "Krähenberg"; Arp et al., 2005), are stromatolites or microbial laminites, which would fall under SMF 20 ("laminated stromatolitic bindstone/mudstone") or LMF 11 ("stromatolite bindstone"), respectively. Even if these structures are laminated, they clearly do not match the laminated dolomudstone described here, which are not microbially induced, but demonstrably the result of physical transport, representing upward decreasing water energy, perhaps in combination with episodic production of authigenic carbonate upon changes in salinity, alkalinity and/or temperature (cf. Rieder et al., 2019). Also, unlike the laminated dolomudstone, stromatolites were reported from the Red Series, which makes sense, as they would typically form under shallow, evaporative conditions.

Sample	Position (m)	Description	$\delta^{13}C$ (‰ VPDB)	$\delta^{18}O$ (‰ VPDB)
AH 17-1	0.33	laminated	-1.51	-3.05
AH 17-1	0.33	homogeneous	-1.58	-3.00
AH 17-1	0.33	laminated	-1.56	-2.81
AH 17-2	1.15	homogeneous	-1.58	-2.24
AH 17-3a	1.8	laminated	-2.16	-2.56
AH 17-3c	1.8	mudclasts	-2.78	-2.21
AH 17-3c	1.8	mudclasts	-2.85	-1.93
AH 17-4b	2.5	mudclasts	-2.19	-1.83
AH 17-4b	2.5	mudclasts	-2.24	-2.22
AH 17-4c	2.5	laminated	-2.22	-3.24
AH 17-4c	2.5	homogeneous	-2.27	-1.31
AH 17-4c	2.5	mudclasts	-2.17	-2.69
AH 17-30a	5.02	peloidal	-1.36	-0.90
AH 17-30a	5.02	peloidal	-1.66	-4.50
AH 17-30c	5.02	peloidal	-1.33	-2.40
AH 17-30c	5.02	peloidal	-1.70	-3.98
AH 17-35o	13.9	laminated	-3.03	-6.25
AH 17-35o	13.9	laminated	-1.94	-3.83
HR 17-1a	0.05	mudclasts	-3.66	-2.01
HR 17-1b	0.05	mudclasts	-4.28	-1.86
HR 17-1b	0.05	mudclasts	-3.64	-0.07
GLS 17-1	-	homogeneous	-2.91	-0.76
GLS 17-4	-	homogeneous	-1.84	-2.04
GLS 17-4	-	homogeneous	-1.74	-1.66
GLN2 17-1	-	homogeneous	0.02	-1.44
GLN2 17-2	-	homogeneous	0.08	-1.53
GLN2 17-3	-	homogeneous	1.39	0.35

Table 2: $\delta^{13}C$ and $\delta^{18}O$ values in micro-drilled carbonate samples of the Arnstadt Formation from Altes Holz, Hottenrode, and Burg Gleichen sections.

Dolowackestone contains mudclasts, which themselves fall into SMF 23 (the homogenous micrite described above). This accurately describes the homogeneous micrite matrix as well as the homogenized mud from which the mudclasts were reworked. This may well match with a shallow lake setting where the sediment is mixed by wave action. However, somewhat higher water energies were probably necessary to rip up mud clasts from the sediment surface, as can be well observed above erosion surfaces (e.g., Figs 5c, d). For a lake system, LMF 3 ("Lime mudstone and wackestone with leaves of plants accumulated on bedding planes") may apply. Indeed, plant debris is observed, and a cm-thick coal bed occurs below the conglomerate layer at Hottenrode. LMF 3 "characterizes a quiet-water far-shore or near-shore environment", but episodic, high water energy is necessary to rework and transport mudclasts, which would be better reflected by LMF 4 ("inhomogeneous fine-bedded intraclast wackestone characterized by reworked laminated mudstone of LMF 2 and nektonic fossils"; Fig. 10c). LMF 4 indicates "nearshore and shore lake-floor areas affected by waves", while the scarcity of fossils may be explained by the water chemistry under ephemeral lake conditions.

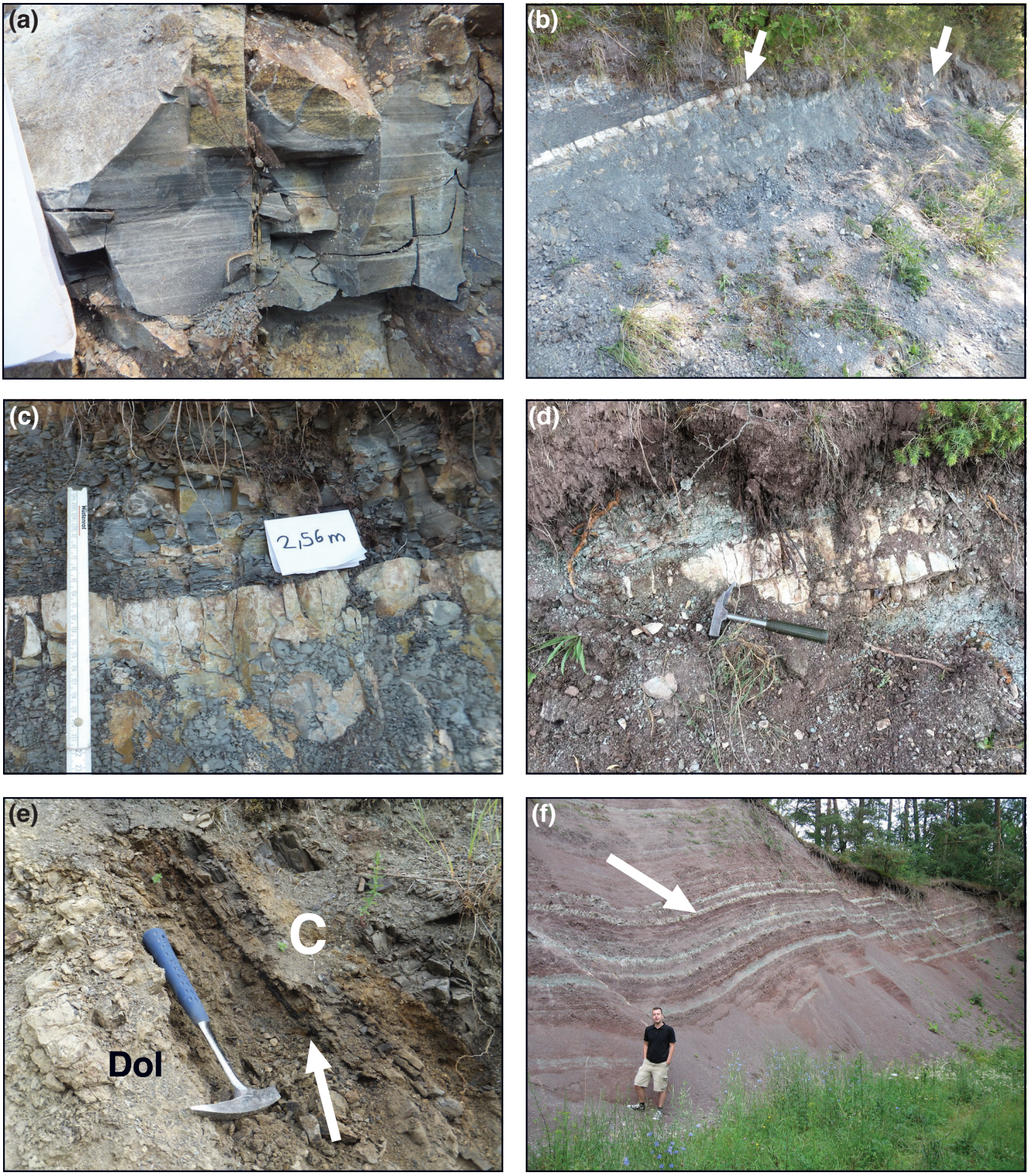

Figure 3: Outcrop photographs of measured stratigraphic section locations: (a) Laminated dolomite-rich claystone at 0.65 m in the section of Altes Holz, Bornhagen (image is ca. 5 cm high). (b) Dolomite beds and 1.8 and 2.56 m in the section of Altes Holz. (c) Close-up of dolomite bed at 2.56 m shown in (B), with sharp transition to laminated dolomitic claystone. (d) Homogeneous dolomite bed at 5.02 m at Altes Holz embedded in greenish shale (at the base of the Upper Red Series). (e) Close-up of Hottenrode section, showing a black organic carbon-rich layer (arrow) and the dolomite conglomerate above (letter C in the image). (f) Outcrop at Krauthausen showing bedding in red and green shale of the Lower Red Series. Arrow indicates dolomite bed.

There is probably a gradual transition to SMF 24 ("lithoclastic floatstones, rudstones and breccias"), the endmember of which is represented by the up to 20-cm-thick dolomite conglomerate in the Hottenrode section (see Arp et al., 2005). Up to several centimetre-sized well-rounded carbonate mudclast occur along with detrital minerals and bioclasts, including vertebrate bones and fresh-water shark teeth (Arp et al., 2004). Also, cross-bedded, elongated micrite clasts (flat pebbles) are observed. SMF 24 pertains to "lag deposits in tidal channels and on tidal flats"

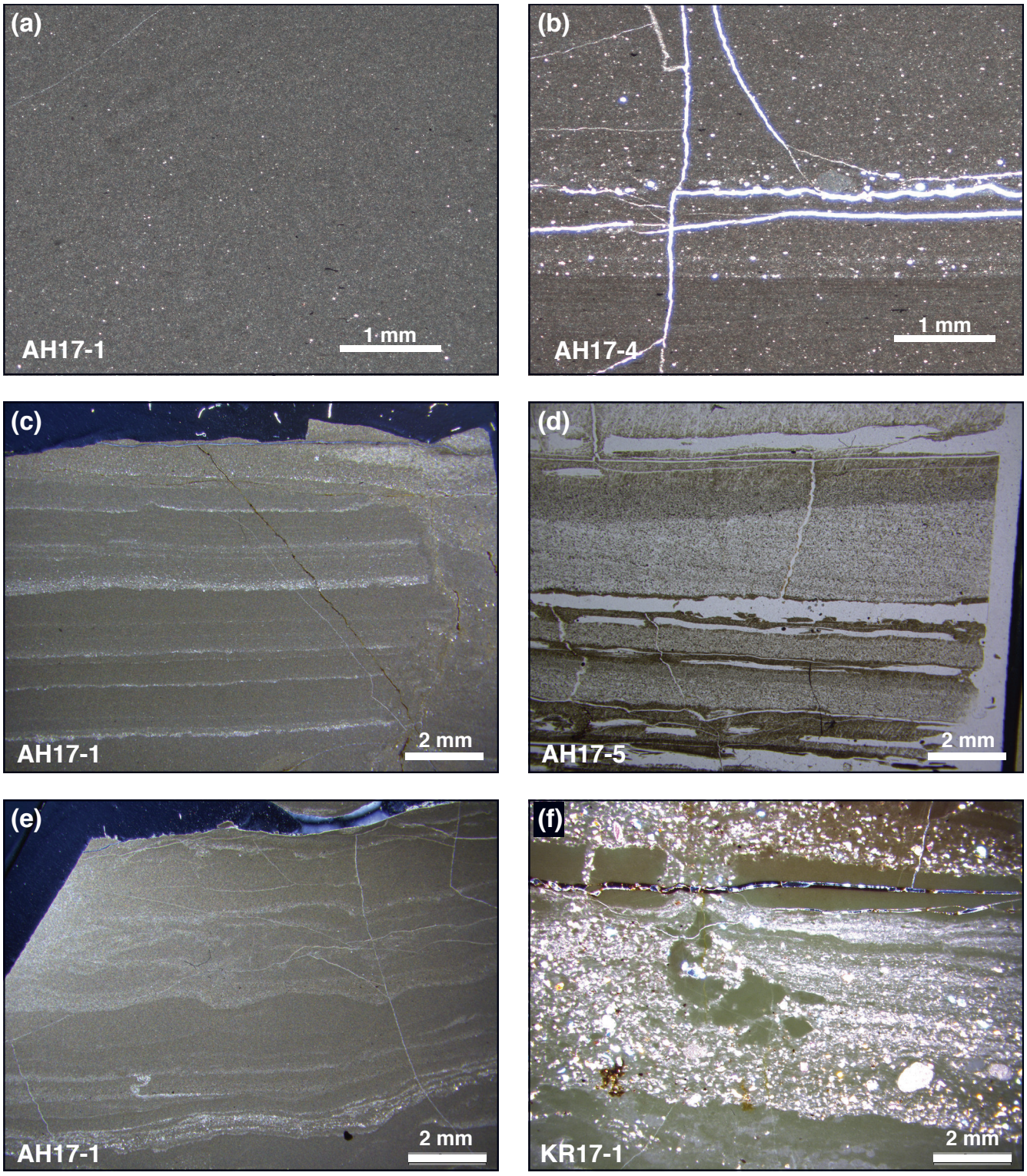

Figure 4: Thin section micrographs of homogeneous and laminated dolomudstone: (a) Homogenous dolomicrite in cm-thick lamina of dolomitic clay (Altes Holz, 0.3 m); (b) laminated dolomudstone showing faint lamination in the bottom part and graded bedding in the upper part, within a homogeneous dolomite bed (Altes Holz, 2.5 m); (c) graded lamination with detrital silt at the base (same sample as in A); (d) sandstone showing cross-bedding (Altes Holz, 3.9 m); (e) slumping structure in a laminated dolomite; same sample as in (a); (f) Teepee structure in laminated dolomite with detrital interlayers in dolomite bed (Krauthausen, 5.6 m).

in the interior of the platform. The corresponding limnofacies would be LMF 13 ("Lithobioclast rudstone composed of reworked, poorly sorted and sometimes strongly rounded carbonate lithoclasts and worn fossil fragments"). Also, this microfacies implies "storm deposits".

Ooids and oncoids are rare in the studied samples. Rare oncoids have been reported from the conglomerate in the Hottenrode section (Arp et al., 2005). Nevertheless, ooid or oncoid packstone occurs in the dolomite layer in the Krauthausen succession. LMF 10 would comprise

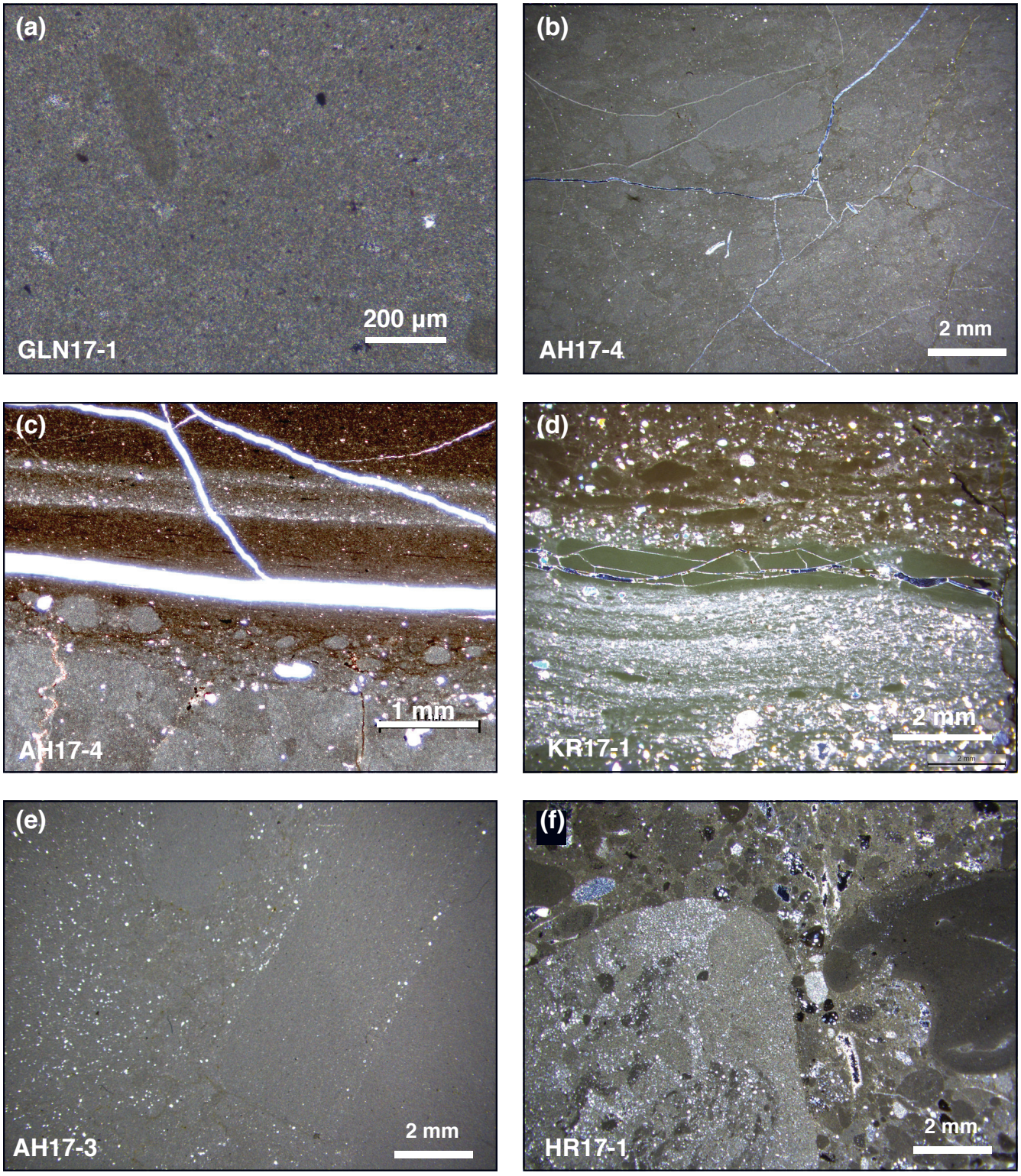

Figure 5: Thin section micrographs of mudclast wackestone consisting of dolomite: (a) Mudclasts in micritic matrix from dolomite at Burg Gleichen; (b) Nodular dolomite, matrix supported, from dolomite bed at Altes Holz, 2.5 m; (c) Erosion surface showing rounded mudclasts ripped up and reworked from the underlying lamina (same sample as in B); (d) Reworked flat pebbles embedded together with detrital silt, dolomite bed at Krauthausen, 5.6 m; (e) Flat pebble showing faint lamination in dolomite bed at Altes Holz, 1.8 m. (f) micritic clasts and dolomite rhomboids from the Hottenrode conglomerate (polarized light).

"oncoid floatstone, packstone and wackestone", which indicates "near-shore and shore areas" and in the case of large oncoids "higher-energy fluvial-lacustrine and brackish-water settings", which all could be accommodated by the above-mentioned mudclast facies. These conditions would reflect a shallow-water environment, which is consistent with the occurrence of oncoids/ooids within the Lower, resp., Upper Red Series.

For the peloidal grainstone found in one dolomite bed in the Upper Red Series in the Altes Holz section, marine

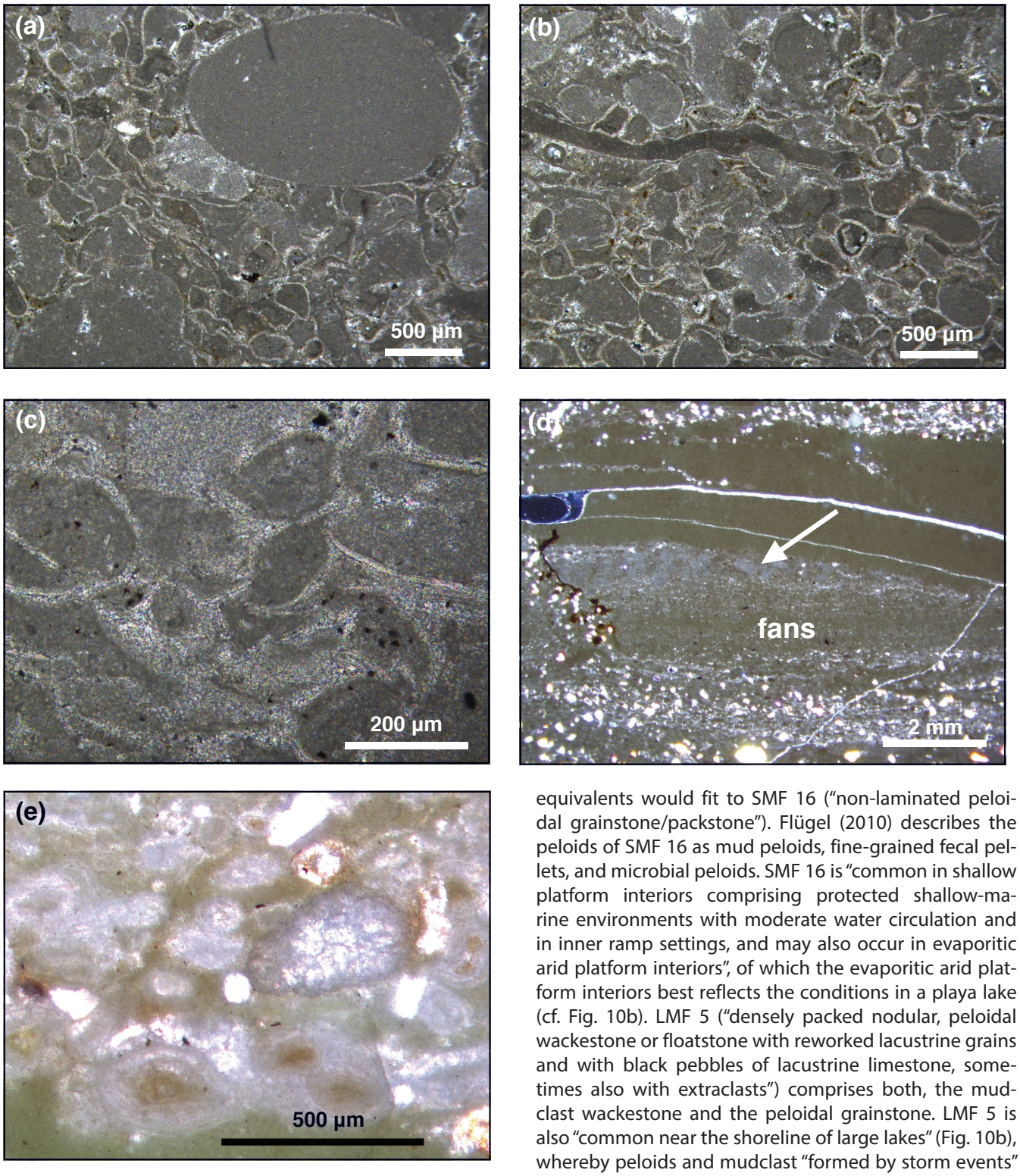

Figure 6: Thin section micrographs of peloidal dolomites: (a) Different types of micritic peloids in dolomite bed from Altes Holz, 5.02 m, showing densely packed structure and deformation due to compaction. Matrix is almost entirely absent, but grains are surrounded by fine cement rims. (b) Some elongate several mm-size features (flat pebbles) are also surrounded by the cement rim. (c) Closeup of peloidal structure showing homogenous micrite peloids surrounded by partially broken isopacheous cement rims. (d) Micritic peloids showing amalgamation (arrow) and cementation by superimposed crystal fan structure (indicated as "fan") in the dolomite bed from the Krauthausen outcrop, 5.6 m. (e) Lamina consisting of ooids or oncoids in the same bed as in (d).

equivalents would fit to SMF 16 ("non-laminated peloidal grainstone/packstone"). Flügel (2010) describes the peloids of SMF 16 as mud peloids, fine-grained fecal pellets, and microbial peloids. SMF 16 is "common in shallow platform interiors comprising protected shallow-marine environments with moderate water circulation and in inner ramp settings, and may also occur in evaporitic arid platform interiors", of which the evaporitic arid platform interiors best reflects the conditions in a playa lake (cf. Fig. 10b). LMF 5 ("densely packed nodular, peloidal wackestone or floatstone with reworked lacustrine grains and with black pebbles of lacustrine limestone, sometimes also with extraclasts") comprises both, the mudclast wackestone and the peloidal grainstone. LMF 5 is also "common near the shoreline of large lakes" (Fig. 10b), whereby peloids and mudclast "formed by storm events" or flood events. In addition, high concentration due to strong evaporation may have caused incrustation of the peloids with a carbonate cement rim, and the crystal fans observed at Krauthausen.

5.2 Meteoric influence, evaporation, and cyclicity

Further information on the palaeo-environment can be gained from trends in C- and O-isotopes. Oxygen isotope values between -5.21 and -0.36‰ (VPDB) are less

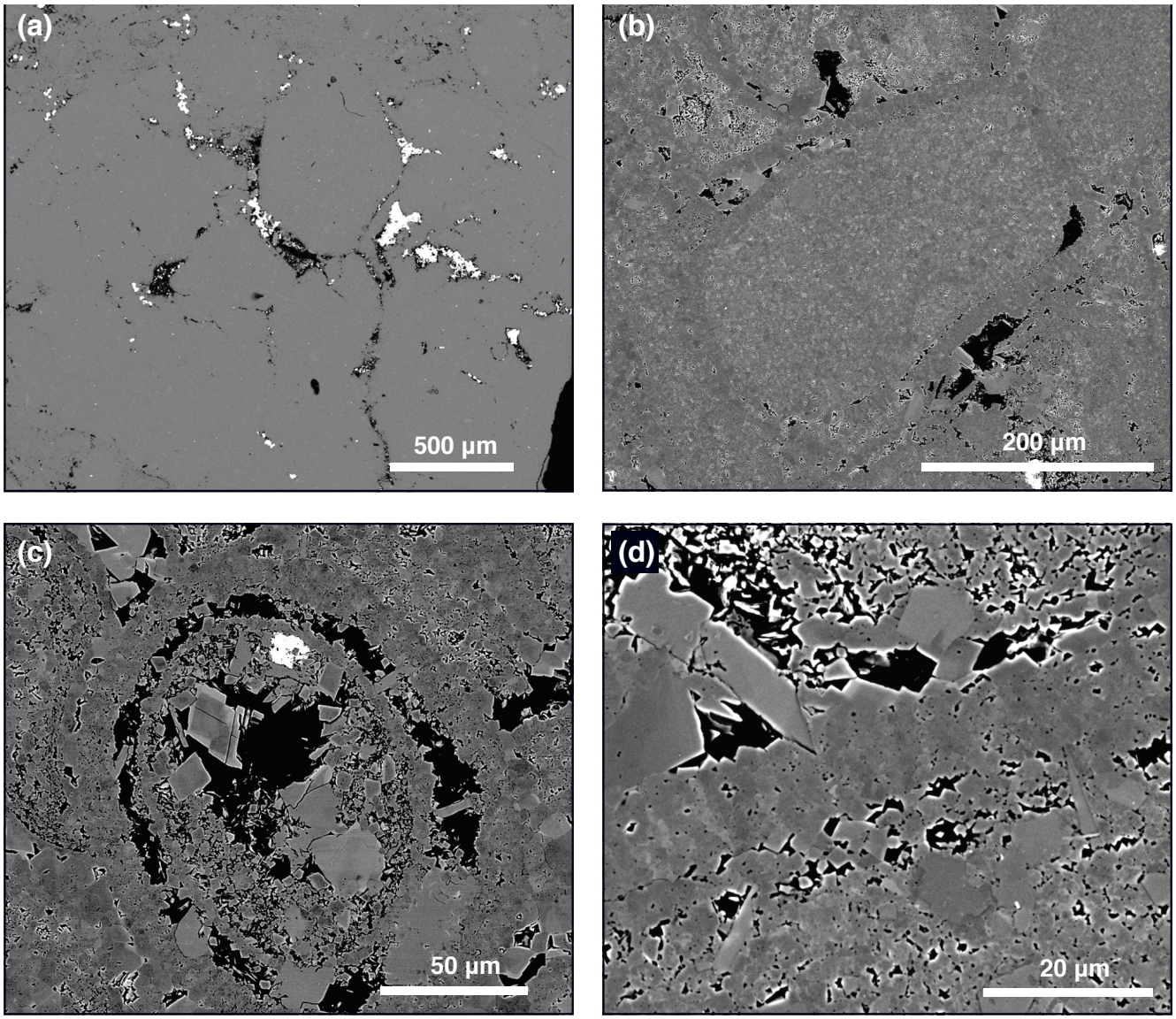

Figure 7: SEM images of polished thin sections of sample AH17-30 (Altes Holz section, 5.02 m) analysed in backscatter mode: (a) Grain supported peloidal structure with barite in the interstices (Ba and S was revealed by EDX in the light-coloured phase). (b) Amplified backscatter contrast reveals internal structure of the peloids. (c) At high magnification, radial crystal arrangement in isopacheous cement rims is visible. (d) Detail of isopacheous cement rim.

negative than expected for carbonate precipitated from meteoric water in an endorheic basin (even if the fractionation effect between water and mineral is taken into account; Vasconcelos et al., 2005). The original $\delta^{18}O$ values would have been even more positive, if the dolomites were partially affected by recrystallization during burial (re-equilibration would result in 7.4‰ more negative values, assuming a burial depth of 1400 m, a geothermal gradient of 30°C/km, and the fractionation factor of Vasconcelos et al., 2005). Hence, the measured value can only be explained by the influence of evaporation. Generally, in the cross-plots a trend from more negative values to more positive values in both C- and O-isotopes are observed (grey arrow in Fig. 9), indicating a humid-arid variation, with humid intervals not only showing a stronger meteoric influence but also more negative carbon isotope values due to organic carbon weathering from soils (Talbot, 1990; Reinhardt and Ricken, 2000b; Arp et al., 2005). No clear trend in $\delta^{18}O$ through the stratigraphic sections can be observed based on the limited dataset, in particular not between dolomite occurring in the Grey and the Red Series.

More insightful are the isotopic trends if they are considered for the different microfacies types separately. Peloidal dolomites in one bed from the Red Series at Altes Holz show variable $\delta^{18}O$ values but rather constant $\delta^{13}C$ values (green arrow in Fig. 9), indicating a pure evaporation trend, while the carbon source remained unchanged. $\delta^{13}C$ values may not necessarily vary with evaporation, depending on the conditions of the carbonate system (cf. Leng and Marshall, 2004). The variation in $\delta^{18}O$ would be consistent with a shallow-water, evaporative environment as indicated by the peloidal mudstones. The carbonate cement rims, which formed

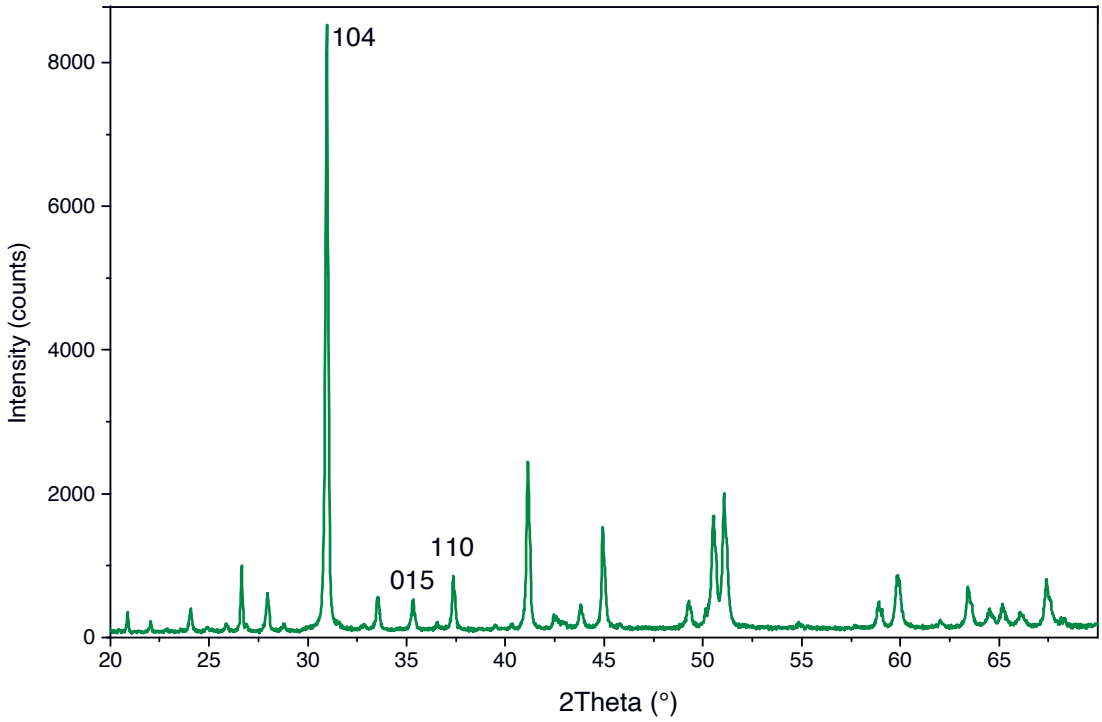

Figure 8: X-ray diffractogram of sample AH17-30 from Altes Holz section showing dolomite as single carbonate phase and minor other minerals such as quartz, feldspar and mica.

early, when the micrite peloids were still unlithified, are most likely also the result of high supersaturation during an episode of strong evaporation. The fact that evaporites are rare in the Arnstadt Formation (e.g., Arp et al., 2005; Reinhardt and Ricken, 2000b) does not rule out that episodically high evaporation and evaporite formation could have occurred. In contrast to the underlying Gipskeuper (Weser Formation; Beutler, 2005), high evaporation may only have prevailed shortly, so that the evaporites get dissolved during the subsequent humid period. Residual beds of former evaporite (i.e., gypsum) nodules are known from both the Lower and the Upper Red Series. Also, barite would indicate the presence of a former evaporite, of which the sulphate would be preserved in barite.

In contrast to peloidal dolomites, $\delta^{13}C$ and $\delta^{18}O$ values cluster closely together in laminated mudstones and mudclasts only show a variation of $\delta^{13}C$ while the $\delta^{18}O$ values remain constant (green arrow in Fig. 9). Isotopically light carbon may be derived from organic matter degradation, whereby an inverse correlation observed in some homogeneous dolomites may suggest a decoupling of organic carbon input from the meteoric-evaporative trend. A similar trend is indeed observed in primary dolomites from the Nördlinger Ries (Arp et al., 2017; see discussion below). It seems that deeper-water settings show less variation of $\delta^{18}O$, probably due to the buffering effect of a larger water body.

Overall, authigenic carbonates may have formed in diverse environments, but all are related to somewhat evaporative conditions and high supersaturation. Figure 10 displays how the different microfacies types fit into the larger context of the basin, in relation to different stages and cyclicity. In the Red Series, conditions were entirely dry, with siliclastic sedimentation due to sheet floods (Fig. 10a), while carbonate deposition only occurred during episodes of higher water supply (Reinhardt and Ricken, 2000b). In those stages (Fig. 10b), the conditions may have been playa-like with a very shallow water column and a high effect of evaporation on isotopic compositions. In contrast, in the Grey Series (Arp et al., 2005), deep water may have persisted, while the carbonate deposition became enhanced during more evaporative episodes, with higher concentration of the brines (Fig. 10c). As we know from modern lakes, such conditions may also prevail in deep water (e.g., Lake Van, McCormack et al., 2018).

5.3 Biogeochemical processes and early diagenesis

Carbon isotope values in the range of -4.28 to 1.39‰ VPDB, with most values between -1.3 and -2.3‰, are near to $\delta^{13}C$ values of bicarbonate in equilibrium with atmospheric CO_2 (around 0‰; e.g., Hollander and McKenzie, 1991). Negative $\delta^{13}C$ values are generally caused by the influence of remineralized organic carbon. A clear negative trend occurs in mudclast-rich sediments. Darker clasts show more negative $\delta^{13}C$ isotope values, suggesting that they formed under more reducing conditions in more organic carbon-rich sediment. The most negative $\delta^{13}C$ values occur in the dolomite conglomerate at Hottenrode. This conglomerate contains dark grey pebbles, most likely eroded and reworked from organic carbon-rich carbonate mud, where the organic matter provides a source of isotopically light carbon.

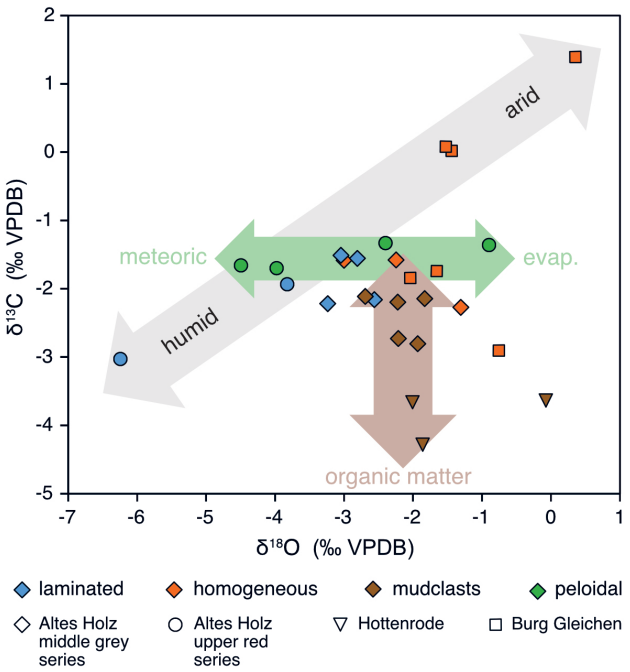

Figure 9: Crossplot of isotopic values ($\delta^{18}O$ against $\delta^{13}C$) measured in micro-drilled carbonates of the Arnstadt Formation. Laminated dolomite values of $\delta^{13}C$ cluster together; other values plot over a wider range of values and show no trends.

The $\delta^{13}C$ signature of organic carbon may have been partially incorporated into the carbonate during early diagenesis (e.g., Heimhofer et al., 2017). Usually, $\delta^{13}C$ in porewater rapidly decreases with depth due to dissimilatory microbial activity (with $\delta^{13}C$ showing a diffusive mixing hyperbola between lake- and porewater; Meister et al., 2019; Meister and Reyes, 2019), and the micrite would partially adopt the negative signature upon lithification or recrystallization. The variability in isotopic composition between different mud clasts supports that carbon isotopes were not caused by a pervasive uniform burial overprint, but occurred during or soon after deposition of the carbonate. Inhomogeneities arise were organic carbon-rich mudclasts are reworked and embedded in a matrix of less organic carbon-rich mud. Alternatively, the DIC in the water column could have been influenced by organic matter degradation in brackish and palustrine environments, so that isotopically light carbon is incorporated into the authigenic carbonate.

The discussion above shows that diverse microfacies occur in the Arnstadt Formation. In particular, the Grey Series represents a perennial lake system with possibly higher water depth and moderate salinities (Arp et al., 2005), that may have resembled some of the modern analogues. Indeed, dolomite formation is also observed in brackish and deep-water lakes (see McCormack et al., 2018; Fussmann et al., 2020), which are only partially (seasonally) evaporative but reach a high carbonate supersaturation. As carbonate precipitation and ripening occurs over extended time periods in the water column or near the sediment/water interface (see discussion below), these carbonates will also become endowed with a negative carbon isotope signature.

Even modern playa lakes show local areas with less saline conditions and abundant biomass production. For example, Deep Springs Lake, California, shows several fresh water springs along its shore, maintaining more swamp-like conditions (Meister et al., 2011). The fine dolomite mud below the surface is black and shows strong sulphate-reducing activity. In this case, however, the negative isotopic signature is not visible in the authigenic carbonate, because the DIC concentration is very high (>500 mmol/l), so that it is barely influenced by the small amounts of organic matter degraded (see Meister et al., 2011).

Overall, the carbon isotope distribution fits well to the facies distribution in the Arnstadt Formation, where uniform values (i.e., more or less in equilibrium with the atmosphere) occur in playa lake deposits, whereas more negative $\delta^{13}C$ values occur in organic matter rich deposits under deeper and/or more brackish water conditions.

5.4 Potential pathways of authigenic carbonate formation

While homogeneous aphanitic dolomite is also observed in diagenetic carbonates, graded bedding provides clear indication for deposition of fine authigenic carbonate mud at the sediment surface. Furthermore, deformation of the laminae, rip-up clasts and rounded mud clasts are clear indication that the sediment was initially not lithified. Brittle deformation with angular clasts and flat pebbles may also result from cohesion of clay-sized carbonate and clay particles and, thus, does not contradict that the sediment was unlithified. The consistency would have been similar to a Greek-style yoghurt. These observations suggest that the sediments were deposited as fine mud. The mudclasts have been reworked and were themselves deposited within fine mud elsewhere. Fine-grained mud was most likely precipitated in the oversaturated lake water and slowly settled from the suspension.

Densely packed peloidal grainstone observed in the dolomite bed in the Upper Red Series of the Altes Holz section are well sorted and well rounded, suggesting a transport process. The peloids, but also some larger mudclasts and flat pebbles in the same sample, are equally surrounded by an isopachous cement rim. During compaction the peloids experienced ductile deformation, while being collapsed into the formerly open porespace; but the hard cement shells around the pebbles were broken apart. This indicates that the interior of the peloids was not lithified yet, while the porespace between the peloids was still empty. The cement rims must therefore have formed before compaction, and it might even be possible that the peloids with rims were transported and winnowed, which would explain their well-sorted size distribution. Clearly, the cement rims have resulted from a precipitation event, from oversaturated lake water. SEM analysis showed that the cement shows radial arrangement of crystals, similar to ooids, but in most cases not showing multiple concentric cement rims. In contrast to the peloids, the ooids and oncoids (only rarely found in the studied samples) were

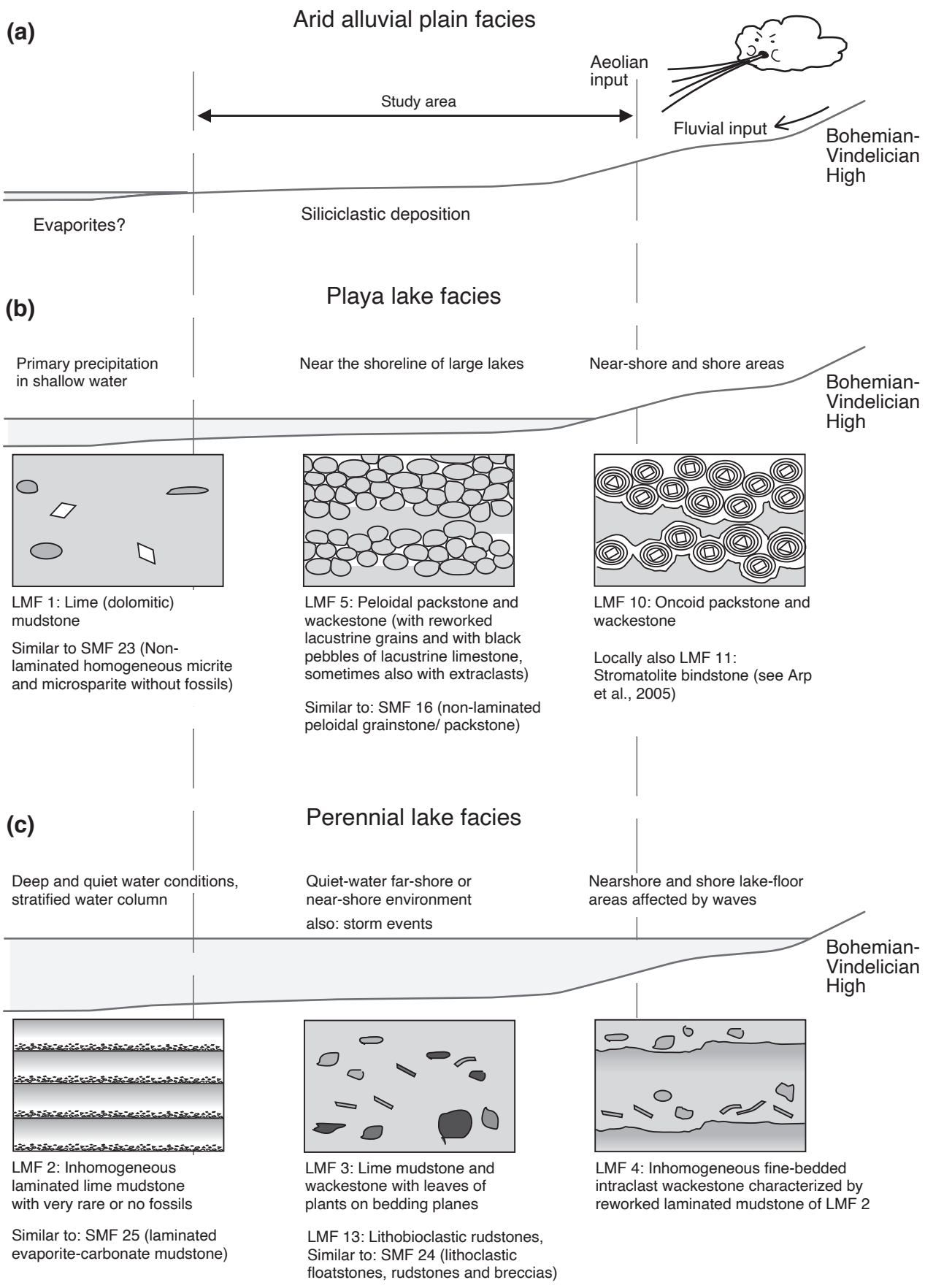

Figure 10: Environmental reconstruction for (a) perennial lake, (b) playa lake and (c) arid mud plain facies in the Germanic Basin during the time of deposition of the Arnstadt Formation. The different standard microfacies (SMF) and limnofacies (LMF) types are indicated.

entirely lithified, such that the interparticle pore space was preserved and later filled with diagenetic cement (cf. ooids in the Lehrberg Beds; Seegis, 1997).

If authigenic carbonate was directly precipitated out of the lake water, the question would be what their original mineralogy was. While X-ray diffraction confirms that all dolomite in the Arnstadt Formation is stoichiometric and well ordered, and no calcite is present, we do not know whether the initial authigenic carbonate was already dolomite. Comparison with modern ephemeral lakes shows that a large spectrum of primary authigenic Ca/Mg-carbonates are commonly formed, such as nearly ordered dolomite (protodolomite) in Holocene Lake Neusiedl, Austria (Neuhuber et al., 2015; Fussmann et al., 2020), and many endorheic and coastal ephemeral lakes worldwide (cf. compilation in Last, 1990), whereas in Deep Springs Lake, California, primary well-ordered dolomite is formed (Peterson et al., 1963; Clayton et al., 1968; Meister et al., 2011). An ephemeral playa lake comparable to modern Deep Springs Lake may have occurred temporarily within an arid distal fluvial plain during deposition of the Upper Red Series, which could have produced dolomite.

A deeper basin probably existed during deposition of dolomitic marl and laminated dolomites in the Middle Grey Series. Nevertheless, the latter situation would not be inconsistent with an evaporative lake scenario, and there is a modern analogue, Lake Van, Turkey, showing deposition of modern fine-grained dolomite mud in deep water (McCormack et al., 2018). Furthermore, Lake Neusiedl is a shallow brackish lake, showing the formation of different Mg-calcites and nearly ordered dolomite (Fussmann et al., 2020). Neuhuber et al. (2015) has demonstrated by ^{14}C dating that dolomite at the sediment surface is several hundred years old. It may therefore have been resuspended and remained in contact with the lake water for a long time. In both cases, Lake Van and Lake Neusiedl, it was proposed that initial disordered Mg/Ca carbonate ripens to dolomite under fluctuating conditions. Intriguingly, Deelman's (1999) experiments suggest dolomite formation under fluctuating conditions, as pertaining to Ostwald's step rule, where the metastable phase (e.g., a disorderd Mg/Ca-carbonate) forms faster under high supersaturation, and this phase ripens to the stable phase (e.g., dolomite) under low supersaturation (Meister, in press). High fluctuation in supersaturation could be imposed by seasonally humid and arid conditions in evaporative lake environments (Meister and Frisia, 2019). Variations in climate and hydrology are implied on different levels based on the microfacies distribution (cf. hierarchy of cyclicity proposed by Reinhardt and Ricken, 2000b). Alternatively, fluctuating conditions may also be imposed at the sediment/water interface, due to lower pH as result of organic acids and microbial fermentation (Fussmann et al., 2020).

The primary formation of Mg/Ca-carbonates and dolomite have become an exciting field of research in recent time, as different pathways for nucleation and growth are being suggested. Observations of shallow marine dolomite from the Carnian Travenanzes Formation (northern Italy; Preto et al., 2015) showed nanocrystal structures where the few-nanometre-scale crystallites show lattice mismatch between each other. This finding was interpreted as indication that dolomite formed via the aggregation of nanocrystals. Such a pathway has also been suggested for Norian platform dolomite in the Dolomia Principale (Southern Alps; Meister and Frisia, 2019) and essentially has been postulated based on laboratory experiments (Rodriguez-Blanco et al., 2015). Whether similar structures occur in dolomites of the Arnstadt Formation remains to be further investigated by HR-TEM analyses. The observations of unlithified fine-grained Ca-Mg-carbonate mud deposited in an evaporative lake setting would be consistent with a primary pathway.

6. Conclusions

Dolomite beds intercalated in clay- and siltstones of the Norian Arnstadt Formation were deposited as authigenic mud of Mg/Ca-carbonate in an extended playa-lake/perennial-lake system, which occurred temporarily in the Germanic Basin. Diverse carbonate microfacies reflect variable environmental conditions with deeper and shallower water, and episodically enhanced supersaturation, due to evaporative conditions. Homogeneous mud was most likely deposited episodically under shallow playa-lake or ephemeral lake conditions, under otherwise dry conditions of the Red Series, while the mud was homogenized due to resuspension by wave action. Laminated carbonates may have been deposited in somewhat deeper water during the deposition of the Grey Series, under calm conditions, while receiving episodic detrital input. In contrast, mud clasts were reworked from the sediment surface at erosional surfaces under higher water energy, i.e., in shallow parts of the lake or along the shoreline. Also deformed laminae and flat pebble layers are probably due to high water energy during flooding or storm events (tempestites) or, perhaps, due to gravitative transport on the slopes of the lake bottom. Peloidal dolomites represent well-sorted mud clasts, whereby a cement rim precipitated under episodically high supersaturation of the lake water, during deposition of the Red Series.

Primary precipitation of Mg-Ca-carbonate in the water column and their deposition as fine mud is supported by the observation that the sediment was largely unlithified after deposition. Although it is not known whether this authigenic carbonate was already dolomite, this mode of authigenic carbonate formation resembles carbonate formation in many modern day endorheic and coastal ephemeral lakes, independent of whether it was a deep basin or a shallow evaporative lake. Fluctuating conditions may have supported both precipitation and ripening according to Ostwald's step rule, which is in line with most recent hypotheses suggesting authigenic formation of carbonates via nucleation and aggregation of nanoparticles.

Acknowledgements

We thank Gernot Arp for guiding us to the most relevant outcrops and providing essential information on the Arnstadt Formation. He also provided valuable comments to the manuscript. Caroline Haberhauer and Stefanie Klackl assisted during fieldwork. Claudia Beybel, Leopold Slawek, and Ilka Wünsche are thankfully acknowledged for preparing high-quality thin sections. Beatrix Bethke supported us during laboratory work. The study was partially financed by the European Commission through IEF Project TRIADOL (no. 626025) and Horizon2020 Project ELEMIN (grant no. 746033), and by the Department of Geology at the University of Vienna. We thank Gerhard H. Bachmann for detailed comments to the regional geology and an anonymous reviewer for constructive feedback to our study.

References

Aigner, T., Bachmann, G.H., 1992. Sequence-stratigraphic framework of the German Triassic. Sedimentary Geology, 80, 115–135.

Arp, G., Hoffmann, V.-E., Seppelt, S., Riegel, W., 2004. Trias und Jura von Göttingen und Umgebung. 74. Jahrestagung der Paläontologischen Gesellschaft, 2.-8.10.2004, Exkursion, 6, 147–192, Göttingen (Universitätsdrucke).

Arp, G., Bielert, F., Hoffmann, V. E., Löffler, T., 2005. Palaeoenvironmental significance of lacustrine stromatolites of the Arnstadt Formation ("Steinmergelkeuper", Upper Triassic, N-Germany). Facies, 51(1-4), 419–441.

Arp, G., Hansen, B.T., Pack, A., Reimer, A., Schmidt, B.C., Simon, K., Jung, D., 2017. The soda lake—mesosaline halite lake transition in the Ries impact crater basin (drilling Löpsingen 2012, Miocene, southern Germany). Facies, 63, 1.

Bachmann, G.H., Hiltmann, W., Lerche, I., 2002. Inkohlung des Unteren Keupers in Südwestdeutschland. N. Jb. Geol. Paläont. Abh., 226, 271–288, Stuttgart.

Bachmann, G.H., Geluk, M.C., Warrington, G., Becker-Roman, A., Beutler, G., Hagdorn, H., Hounslow, M.W., Nitsch, E., Röhling, H.-G., Simon, T., Szulc, A., with contributions by Michiel Dusar, M., Nielsen, L.H., Barnasch, J., Franz, M., 2010. Triassic. In: Petroleum Geological Atlas of the Southern Permian Basin Area (Eds J.C. Doornenbal, A.G. Stevenson), 149–173; Houten (EAGE Publications).

Balci, N., Menekşe, M., Karagüler, N.G., Sönmez, M.S., Meister, P., 2016. Reproducing authigenic carbonate precipitation in the hypersaline Lake Acıgöl (Turkey) with microbial cultures. Geomicrobiology Journal, 33, 758–773.

Barnasch, J., 2010. Der Keuper im Westteil des Zentraleuropäischen Beckens (Deutschland, Niederlande, England, Dänemark): diskontinuierliche Sedimentation, Litho-, Zyklo- und Sequenzstratigraphie. Schriftreihe der Deutschen Gesellschaft für Geowissenschaften, 71, 7–169, Hannover. ISBN-10: 3510492188

Barth, G., Franz, M., Heunisch, C., Ernst, W., Zimmermann, J., Wolfgramm, M., 2018. Marine and terrestrial sedimentation across the T-J transition in the North German Basin. Palaeogeogr., Palaeoclimatol., Palaeoecol., 489, 74–94.

Beutler, G., Hauschke, N., Nitsch, E., 1999. Faziesentwicklung des Keupers im Germanischen Becken. In: Hauschke, N., Wilde, V. (eds.) Trias. Eine ganz andere Welt. Pfeil, München, pp 129–174.

Beutler, G., Hauschke, N., Nitsch, E., Vath, U., 2005. Stratigraphy of Germany IV, Keuper (upper Triassic). Curier Forschungsinstitut Senckenberg, 253, 296 pp. Deutsche Stratigraphische Kommission. ISBN 978-3-510-61376-2

Breitenbach, S.F.M., Bernasconi, S.M., 2011. Carbon and oxygen isotope analysis of small carbonate samples (20 to 100 µg) with a GasBench II preparation device. Rapid Commun. Mass Spectrom. 25, 1910–1914.

Clayton, R.N., Jones, B.F., Berner, R.A., 1968. Isotope studies of dolomite formation under sedimentary conditions. Geochim. Cosmochim. Acta, 32, 415–432.

Deelman, J.C., 1999. Low-temperature nucleation of magnesite and dolomite. Neues Jahrbuch für Mineralogie (Stuttgart), Monatshefte, 7, 289–302.

Duchrow, H., 1984. Keuper. Geologie des Osnabrücker Landes. In: Klassen, H. (ed.), Naturwissenschaftliches Museum Osnabrück, 221–334.

Dunham, R.J., 1962. Classification of carbonate rocks according to depositional texture. In: Ham, W.E. (ed.), Classification of Carbonate Rocks. American Association of Petroleum Geologists Memoir, Tulsa, 108–121.

Eugster, H.P., Hardie, L.A., 1978. Saline lakes. In: Lerman, A. (ed.), Lakes, Chemistry, Geology, Physics. Springer-Verlag, New York, N.Y., pp. 237–293.

Eugster, H.P., Surdam, R.C., 1973. Depositional environment of the Green River Formation of Wyoming: a preliminary report. Bull. Geol. Soc. Am., 84, 1115–1120.

Feist-Burkhardt, S., Götz, A.E., Szulc, J., Borkhataria, R., Geluk, M., Haas, J., Hornung, J., Jordan, P., Kempf, O., Michalik, J., Nawrocki, J., Reinhardt, L., Ricken, W., Röhling, H.G., Rüffer, T., Török, A., Zühlke, R., 2008. Triassic. The geology of central Europe, 2, 749–821.

Flügel, E., 2010. Microfacies of carbonate rocks - analysis, interpretation and application. 2nd. Edition, Springer-Verlag Berlin Heidelberg.

Folk, R.L., 1959. Practical petrographical classification of limestones. Amer. Ass. Petrol. Geol. Bull., 43, 1–38.

Franz, M., 2008. Litho- und Leitflächenstratigraphie, Chronostratigraphie, Zyklo- und Sequenzstratigraphie des Keupers im östlichen Zentraleuropäischen Becken (Deutschland, Polen) und Dänischen Becken (Dänemark, Schweden). Dissertation, Martin-Luther University, Halle-Wittenberg.http://sundoc.bibliothek.uni-halle.de/diss-online/08/09H048/index.htm

Friedman, G.M., 1965. Terminology of crystallization textures and fabrics in sedimentary rocks. Journal of Sedimentary Research 35, 643–655.

Füchtbauer, H., Goldschmidt, H., 1966. Beziehungen zwischen Calzium-Gehalt und Bildungsbedingungen der Dolomite. Geologische Rundschau 55, 29–40.

Fussmann, D., von Hoyningen-Huene A.J.E., Reimer, A., Schneider, D., Arp, G., Daniel, R., Babková, H., Peticzka,

R., Maier, A., Meister, P., 2020. Authigenic formation of Mg-Ca-carbonates in shallow alkaline water in Lake Neusiedl, Austria. Biogeosciences 17, 2085–2106. https://doi.org/10.5194/bg-2019-449

Heimhofer, U., Meister, P., Bernasconi, S.M., Ariztegui, D., Martill, D.M., Rios-Netto, A.M., Schwark, L., 2017. Isotope and elemental geochemistry of black shale-hosted fossiliferous concretions (Early Cretaceous Santana Formation, Brazil). Sedimentology 64, 150–167. https://doi.org/10.1111/sed.12337

Hollander, D.J., McKenzie, J.A., 1991. CO_2 control on carbon isotope fractionation during aqueous photosynthesis: a paleo pCO_2 barometer. Geology 19, 929–932.

Iannace, A., Frisia, S., 1994. Changing dolomitization styles from Norian to Rhaetian in southern Tethys realm. In: "A Volume in Honour of Dolomieu" (Eds. B. Purser, M. Tucker, D. Zenger), Int. Assoc. Sedimentol. Spec. Publ. 21, 75–89.

Kellner, A., 1997. Das Typusprofil der Arnstadt-Formation (Steinmergelkeuper, Obere Trias) in Thüringen. Halle/Saale, Martin Luther Universität Halle-Wittenberg.

Korte, C., Kozur, H.W., Bruckschen, P., Veizer, J., 2003. Strontium isotope evolution of Late Permian and Triassic seawater. Geochim. Cosmochim. Acta 67, 47–62.

Kozur, H.W., Bachmann, G.H., 2010. The Middle Carnian wet intermezzo of the Stuttgart Formation (Schilfsandstein), Germanic Basin. Palaeogeogr. Palaeoclimatol. Palaeoecol. 290, 107–119.

Kozur, H.W., Weems, R.E., 2010. The biostratigraphic importance of conchostracans in the continental Triassic of the northern hemisphere. In: The Triassic Timescale (Ed S.G. Lucas), Geological Society London Special Publications, 334, 315–417.

Last, W.M., 1990. Lacustrine dolomite – an overview of modern, Holocene, and Pleistocene occurrences. Earth-Science Reviews, 27, 221–263.

Leng, M.J., Marshall, J.D., 2004. Palaeoclimate interpretation of stable isotope data from lake sediment archives. Quat. Sci. Rev., 23, 811–831.

Lumsden, D.N., 1979. Discrepancy between thin-section and X-ray estimates of dolomite in limestone. J. Sed. Petrol. 49, 429–435.

Machel, H.G., 2004. Concepts and models of dolomitization: a critical reappraisal. Geological Society, London, Special Publications, 235, 7–63.

McCormack, J., Bontognali, T.R.R., Immenhauser, A., Kwiecien, O., 2018. Controls on cyclic formation of Quaternary early diagenetic dolomite. Geophysical Research Letters, 45, 3625–3634.

Meister, P., in press. Ostwald's step rule: a consequence of growth kinetics and nano-scale energy landscape. In: Nucleation and growth of sedimentary minerals (Eds. Meister, P., Fischer, C., Preto, N.); IAS Spec. Publ.

Meister, P., Frisia, S., 2019. Dolomite formation by nano-crystal aggregation in the Dolomia Principale of the Brenta Dolomites (Northern Italy). Rivista Italiana di Paleontologia e Stratigrafia 125, 183–196.

Meister, P., McKenzie, J. A., Bernasconi, S. M., Brack, P., 2013. Dolomite formation in the shallow seas of the Alpine Triassic. Sedimentology 60, 270–291.

Meister, P., Reyes, C., Beaumont, W., Rincon, M., Collins, L., Berelson, W., Stott, L., Corsetti, F., Nealson, K.H., 2011. Calcium- and magnesium-limited dolomite precipitation at Deep Springs Lake, California. Sedimentology 58, 1810–1830.

Meister, P., Reyes, C., 2019. The carbon-isotope record of the sub-seafloor biosphere. In: "Tracking the Deep Biosphere through Time" (Eds. H. Drake, M. Ivarsson, C. Heim), Geosciences 9, 507, 1–25. https://doi:10.3390/geosciences9120507

Meister, P., Liu, B., Khalili, A., Böttcher, M.E., Jørgensen, B.B., 2019. Factors controlling the carbon isotope composition of dissolved inorganic carbon and methane in marine porewater: An evaluation by reactive-transport modelling. J. Marine Systems 200, 103227, 1–18. https://doi.org/10.1016/j.jmarsys.2019.103227

Naumann, E., 1911. Beitrag zur Gliederung des mittleren Keupers im nördlichen Thüringen. Jb. Preuß. Geol. Landesanst., 28, 549–586.

Neuhuber, S., Steier, P., Gier, S., Draganits, E., Kogelbauer, I., 2015. Radiogenic Carbon Isotopes in Authigenic Carbonate from Lake Neusiedl, Austria. Geophysical Research Abstracts, 17, 15399–15399.

Patzelt, G., 1994. Streifzüge durch die Erdgeschichte Nordwest-Thüringens. 1. Aufl., 1-96 S.; Gotha (Justus Perthes Verlag).

Peterson, M.N.A., Bien, G.S., Berner, R.A., 1963. Radiocarbon studies of recent dolomite from Deep Springs Lake, California. J. Geophys. Res. 68, 6493–6505.

Preto, N., Breda, A., Corso, J. D., Spotl, C., Zorzi, F., Frisia, S., 2015. Primary dolomite in the Late Triassic Travenanzes Formation, dolomites, Northern Italy: facies control and possible bacterial influence. Sedimentology 62, 697–716.

Reinhardt, L., Ricken, W., 2000a. Climate cycles documented in a playa system: comparison of geochemical signatures derived from subbasins (Triassic, Middle Keuper, German Basin). Zbl. Geol. Paläont. Teil I, Heft 3-4, 315–340, Stuttgart.

Reinhardt, L., Ricken, W., 2000b. The stratigraphic and geochemical record of playa cycles: monitoring a Pangaean monsoon-like system (Triassic, Middle Keuper, S. Germany). Palaeogeography, Palaeoclimatology, Palaeoecology 161, 205–227.

Reinhardt, L., 2002. Dynamic stratigraphy and geochemistry of the Steinmergel-Keuper playa system: a record of Pangaean megamonsoon cyclicity (Triassic, Middle Keuper, Southern Germany). Dissertation, Geologisches Institut Köln. Köln, Universität Köln, 174.

Rieder, M., Wegner, W., Horschinegg, M., Klackl, S., Preto, N., Breda, A., Gier, S., Klötzli, U., Bernasconi, S.M., Arp, G., Meister, P., 2019. Precipitation of dolomite from seawater on a Carnian coastal plain (Dolomites, northern Italy): evidence from carbonate petrography and Sr isotopes. Solid Earth 10, 1243–1267. https://doi.org/10.5194/se-10-1243-2019

Rodriguez-Blanco, J.D., Shaw, S., Benning, L.G., 2015. A route for the direct crystallization of dolomite. American Mineralogist 100, 1172–1181.

Rosenbaum, J., Sheppard, S.M.F., 1986. An isotopic study of siderites, dolomites and ankerites at high temperatures. Geochim. Cosmochim. Acta, 50(6), 1147–1150.

Schauer, M., Aigner, T., 1997. Cycle stacking pattern, diagenesis and reservoir geology of peritidal dolostones, Trigonodus-Dolomite, Upper Muschelkalk (Middle Triassic, SW-Germany). Facies, 37, 99–113.

Seegis, D., 1997. Die Lehrbergschichten im Mittleren Keuper von Süddeutschland –Stratigraphie, Petrographie, Paläontologie, Genese. Ph.D. Thesis, Univ. of Stuttgart.

Stille, H., Lotze, F., 1932. Geologische Übersichtskarte der Umgebung von Göttingen (Hochschul-Exkursionskarte Nr. 3). Berlin (Preuß. Geol. Landesanstalt).

Stille, H., Lotze, F., 1933. Erläuterungen zur Geologischen Übersichtskarte der Umgebung von Göttingen [Hochschul-Exkursionskarte Nr. 3]: 67 S., 1 Kt.; Berlin (Preußische Geologische Landesanstalt).

Talbot, M.R., 1990. A review of the palaeohydrological interpretation of carbon and oxygen isotopic ratios in primary lacustrine carbonates. Chem. Geol., 80, 261–279.

Trümpy, R., 2006. Geologie der Iberger Klippen und ihrer Flysch-Unterlage. Eclogae geol. Helv., 99, 79–121.

Vasconcelos, C., McKenzie, J.A., Warthmann, R., Bernasconi, S., 2005. Calibration of the $\delta^{18}O$ paleo-thermometer with dolomite formed in microbial cultures and natural environments. Geology, 33, 317–320.

Vollmer, T., 2005. Paleoclimatology of Upper Triassic playa cycles: new insights into an orbital controlled monsoon system (Norian, German Basin). PhD Thesis Univ. Köln. 164 pp.

Warren, J., 2000. Dolomite: occurrence, evolution and economically important associations. Earth-Science Reviews, 52, 1–81.

Yuan, J., Huang, C., Zhao, F., Pan, X., 2015. Carbon and oxygen isotopic compositions, and palaeoenvironmental significance of saline lacustrine dolomite from the Qaidam Basin, Western China. Journal of Petroleum Science and Engineering, 135, 596–607. doi:10.1016/j.petrol.2015.10.024

Ziegler, P.A., 1990. Geological atlas of Western and Central Europe. Shell Internationale Petroleum Maatschappij, Den Haag, 239 pp, 52 encl.

Received: 12.10.2020
Accepted: 29.9.2021
Editorial Handling: Sylke Hilberg